J. Fluid Mech. (1991), *vol.* 230, *pp.* 391–428
Printed in Great Britain

Field measurements of wave-induced pressure over wind-sea and swell

By DIETER HASSELMANN[1] AND JENS BÖSENBERG[2]

[1]Meteorologisches Institut, Universität Hamburg, Bundesstrasse 55, D-2000 Hamburg 13, Germany

[2]Max-Planck-Institut für Meteorologie, Bundesstrasse 55, D-2000 Hamburg 13, Germany

(Received 10 August 1987 and in revised form 1 October 1990)

Results of two field experiments in the North Sea are presented. Pressure was measured at two fixed heights above the mean water level and correlated with simultaneous wave height measurements. Roughly 90 hours of data have been analysed and the results are in agreement with earlier results obtained by Snyder *et al.* (1981). Measurements over swell give no indication of wave decay or growth for waves travelling faster than the wind or against the wind.

1. Introduction

We present the results of two field experiments conducted in 1977 and 1981 in the North Sea to measure the atmospheric pressure over surface gravity waves. We compare our results with those of two recent field experiments, the Bight of Abaco experiment (Snyder *et al.* 1981) and a further North Sea experiment (Hsiao & Shemdin 1983). A preliminary analysis of the 1977 experiment has been given in Hasselmann *et al.* (1986).

Interest in this area arises because the wave induced pressure determines the major part of the energy and momentum flux from the atmosphere to the wave field. Furthermore, the complex boundary-layer flow over waves poses a challenging problem with a long history (Jeffreys 1924; Miles 1957, 1959, 1967; Benjamin 1959; Phillips 1957; Townsend 1972; Gent & Taylor 1976; Gent 1977; Kawai 1979). It continues to attract particularly turbulence modellers, and a few recent papers which can help to backtrack the literature are Al-Zanaidi & Hui (1984), McLean (1983) and Jacobs (1987). Chalikov (1986) gives a review of impressive recent work at Leningrad, in particular we mention Makin (1979, 1980, 1981, 1982, 1983*a*, *b*).

Theory has been compared both with field and laboratory measurements. The latter provide greater precision but doubts remain as to how well they model the field situation, as discussed by Makin & Chalikov (1980) and Chalikov (1986). Laboratory measurements against which theory is often checked, are Kendall (1970), Stewart (1970), Kato & Sano (1971), Shemdin & Hsu (1967), Lai & Shemdin (1971) and Takeuchi, Leavitt & Chao (1977), while some more recent papers with long lists of references are Hsu *et al.* (1982), Young & Sobey (1985), Mitsuyasu & Honda (1982), Papadimitrakis, Hsu & Street (1986) and Papadimitrakis, Street & Hsu (1988). For field experiments the paper by Snyder *et al.* (1981), to which we refer for a detailed summary, brought clarity to a situation confused by conflicting results of earlier experiments of Dobson (1971*a*, *b*), Elliott (1972) and Snyder (1974). Hsiao & Shemdin (1983) report on both velocity and pressure measurements, see also Kondo, Fujinawa & Naito (1972), Hsiao & Shemdin (1983, 1985) and Dobson (1985).

Theories differ as to the way in which turbulence closure is achieved and the corresponding additional boundary conditions are formulated. Most models use second-order closure but there still remains much freedom for variation. The perplexing feature is that all these different approaches yield fairly similar results and a comparison with experiment hardly helps to select the best theory. In any case, however, the theory of Miles (1957, 1959) continues to play its outstanding role as a yardstick and despite its idealizations it has predicted the pressure reasonably well.

The non-dimensional parameters of a linear theory may be chosen to be u_*/c, (kz_0) and $(u_* z_0/\nu)$, $\cos\Theta$, where the notation is standard, i.e.

$$U(z) = \frac{u_*}{\kappa}\log\left(\frac{z}{z_0}\right) \quad \text{for } z > 20\frac{\nu}{u_*}, \quad u_*^2 = -(u_1' u_3'),$$

$$c = \frac{\omega}{k}, \quad \boldsymbol{kU} = kU\cos\Theta, \quad \omega^2 = kg\tanh(kh).$$

We may for the moment disregard $\cos\Theta$, which in fact is absorbed into the product $u_*\cos\Theta/c$ for the Miles (1957) theory. In the laboratory all of these parameters can be made to agree with typical field values, except that kz_0 is usually lower in the field. Experiments in wind-wave flumes should therefore be suited to test both the linear theories which neglect turbulent wave-induced stress (Miles 1957, 1959; Benjamin 1959) and those which include them (e.g. Townsend 1972; Al-Zanaidi & Hsu 1984). For nonlinear theories for example the monomodal version of Gent & Taylor (1976) and Gent (1977) or the multimodal one of Makin (1979, 1980, 1981, 1982, 1983*a*, *b*) and Chalikov (1986) the adequacy of wave flumes becomes more doubtful. It may be argued that we do not yet understand the scaling properties of the problem sufficiently well to explain the good agreement between laboratory and field experiments, and to confidently extrapolate the results of the Bight of Abaco experiment to longer waves and higher windspeeds, while staying in a well-covered range of u_*/c.

This is the most convincing justification for our North Sea experiment, which can be viewed as an extension of the Bight of Abaco experiment to rougher conditions, more typical of those in the open ocean but entailing a rougher, less sophisticated experiment. In terms of non-dimensional parameters the two experiments are similar and the same holds true for the results. We do not attempt to extrapolate to higher windspeeds and longer waves.

For waves outrunning or running against the wind, most theories, except for Miles (1957, 1959) and Benjamin (1959) predict wave damping. Gent (1977) argues that extrapolation of his calculations to very long swell does not contradict the swell propagation measurements of Barber & Ursell (1948), Munk *et al.* (1963) and Snodgrass *et al.* (1966) and the results of Chalikov (1986) and Makin (1980, 1981, 1983*a*, *b*) support his claims. In contrast the damping rates predicted by Al-Zanaidi & Hui (1984) are higher than observed in these swell measurements.

We shall compare our damping rates with some predictions.

2. The experiments

2.1. *Site description, instrument support and logistics*

The first experiment was performed in June 1977, the second at the end of September 1981 as part of the KonTur experiment. Both were conducted in the North Sea at station 8 of the JONSWAP array (K. Hasselmann *et al.* 1973; Günther, Rosenthal &

Richter 1979), approximately 27 km off the island Sylt where the water is about 18 m deep.

Instruments were mounted on the meteorological 'needle'. This consisted of a strong main mast water-jetted into the sand, which was sealed by a flange at the surface and on which a slim mast of 9 m length – the needle – was mounted. Figure 1 shows the upper portion of mast and needle. The mast consisted of cylindrical sections with a maximum diameter of 2.00 m at the sea floor and a minimum one of 0.61 m at the top flange, which was 3.10 m above low tide and 1.10 m above high tide level. The needle's diameter narrowed bottom to top, from 0.30 to 0.20 m. The needle supported spars of about 2 m length on which smaller structures actually carrying the instruments were mounted. The spars could be rotated around the needle for adjustments. The base for maintenance and repair was provided by a larger vessel, in 1977 *RV Gauss* and in 1981 *RV Meteor*, which typically lay about 500 m away from the needle in a cross-wind direction. Connections between Sylt and station 8 were maintained by a smaller boat, *RV Regulus*.

In 1977 data were transmitted in PCM-mode directly from the needle to a land station in Sylt, where the data were monitored and recorded on tape, whereas in 1981 data were telemetered to *RV Meteor* and recorded there. In 1977 tapes were taken to Hamburg and the data were analysed in an extensive quick look on a larger computer in Hamburg. The delay between measurements and quick look results was typically 2 days, and while this is a fairly long time this data control still proved valuable for eliminating sources of error. Because of rough seas the connections between *RV Meteor* and Sylt by *RV Regulus* were too irregular to allow a similar quick look in 1981.

2.2. *Instrumentation*

2.2.1. *Environmental measurements*

In 1977 windspeed was measured with cup anemometers at heights of 1.0, 4.10 and 8.30 m (all heights above the flange) see also figure 1. At 8.50 m there were also a thermometer and a wind direction vane. Water temperature was measured at 2.80 and 3.60 m below the flange.

In 1981 profiles of dry and wet bulb temperatue (5 heights between 7.63 and 1.39 m) and of windspeed (8 heights between 7.13 and 0.94 m) were available. Two wind vanes were mounted at 6.96 and 6.10 m. Water temperature was recorded at 2.80 and 3.70 m below the flange.

All environmental data were sampled at 2 Hz.

2.2.2. *Pressure measurements*

Atmospheric pressure was measured at two heights in 1977; because of hostile conditions only one pressure sensor was operated in 1981. In both experiments the same type of pressure probe was used. These were kindly provided by R. Snyder and are identical in design to those used previously in the Bight of Abaco experiments.

The probes' characteristics were checked in a wind tunnel and apart from minor manufacturing deviations found to agree with those reported by Snyder (Snyder *et al.* 1974). In particular the pressure coefficient μ_p is less than 0.02 for angles of attack less than 18° and windspeeds between 4 and 16 m/s. For lower wind speeds, $U \sim 1.5$ m/s μ_p increases to 0.03. Snyder *et al.* (1981) report $|\mu_p| < 0.02$, whereas in previous experiments Snyder used an even better probe $|\mu_p| < 0.01$ (figure 1 of Snyder *et al.* 1974). However, even with our slightly larger coefficients at lower wind speeds the errors so introduced remain negligible.

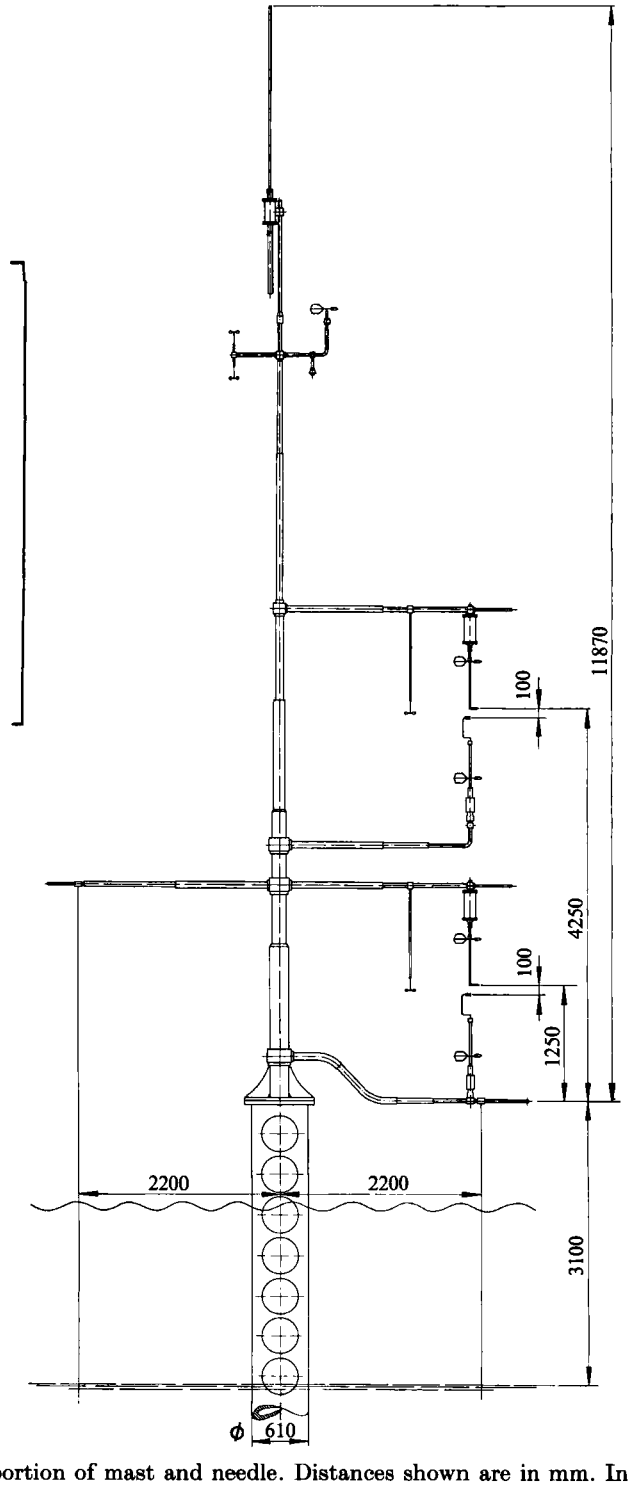

FIGURE 1. Upper portion of mast and needle. Distances shown are in mm. In this case pressure sensors are in hanging position on the top and second spar. Just under the pressure sensor are three-dimensional hot-film anemometers (not treated) and closer to the mast are cup anemometers. The two resistance wires are also shown. A cup anemometer, a wind vane and two thermometers are close to the top of the needle, to which is fastened the transmitting antenna.

The pressure transducer was a Digiquartz (Model 215-A, Paro Scientific Sales Inc). Signal processing with specifically developed high-frequency electronics led to absolute (rather than differential) pressure measurements with a resolution of 0.05 Pa. Laboratory tests showed the system to be stable with negligible drift over periods in the order of 10 h. Over longer periods a drift in the order of 30 Pa/month (at mean values of 10^5 Pa) was detected.

The assembled system, consisting of sensor, connecting pipe and transducer, was dynamically calibrated against a Barocel Type 581 fast response differential pressure gauge. For frequencies below 5 Hz the transfer function is flat and the phase shift less than 0.3°. To prevent stalling the pressure probes were mounted on adequately responding wind vanes, thus limiting the angle of attack to small values (probably less than 10°). The entire arrangement is shown in figure 2. The vane assembly resembles Snyder's (Snyder *et al.* 1974); we used a magnetic fluid instead of mercury as a sealing fluid.

The probes could be mounted at several heights and could be mounted at any of the positions occupied by fluctuation sensors in figure 1, at 4.25 m, 4.15 m, 1.25 m and 1.15 m above the flange. In addition, it was possible to hang the probe from the lowest spar, so that the height of 1.15 m below the flange was also available. In 1977 a typical height above the mean surface was 2 m, while in 1981 it was 6 m. The lowest height in 1977 was 0.75 m and experience showed that owing to spray, or even simply high waves, good measurements were hard to obtain at lower levels.

All atmospheric pressure data were sampled at 10 Hz.

2.2.3. *Wave measurements*

In 1977 wave information was obtained from 2 resistance wires, an underwater pressure sensor and a pitch and roll buoy, while in 1981 only two resistance wires were operating. The underwater pressure sensor was mounted close to the mast; the radial distance was 20 cm to the mast and the vertical position 3.60 m below the flange. The pressure was sampled at 10 Hz. The pitch and roll buoy was operated entirely independently of the needle system and the two systems were unsynchronized. The horizontal separation between the pitch and roll buoy and the needle was about 500 m; the buoy was deployed from *RV Gauss*, where the data were recorded on tape. For various reasons not all needle data were supplemented by pitch and roll data. The resistance wires were fastened to diametrically opposed spars and kept taut by a weight. Ideally, one of the wires would hang vertically beneath the pressure sensors. In 1977 the wires were observed to slant occasionally owing to the drag of the current. We were unable to measure the displacement of the wire from its ideal position or even to regularly estimate it by eye. On one occasion the displacement was estimated to be rather large, about 0.30 m. In 1981 special attention was given to the slant of the wires on every maintenance inspection and this time no displacement as large as in 1977 was observed. The reason for this difference is unknown.

The resistance wires produced two output signals, a 10 Hz output, which we did not use, and a 2 Hz Butterworth filtered series. The electronic filters were tested before and after the experiment and found to have remained stable. Cross-comparisons between the wires and the underwater pressure sensor did show, however, that the gain of the entire resistance wire system would sometimes drift by a few per cent over a period of hours, but this type of error did not accumulate over the entire length of the experiment. Furthermore, the total variance (ζ^2) of the two resistance wires would sometimes differ by as much as 10% even for new wires.

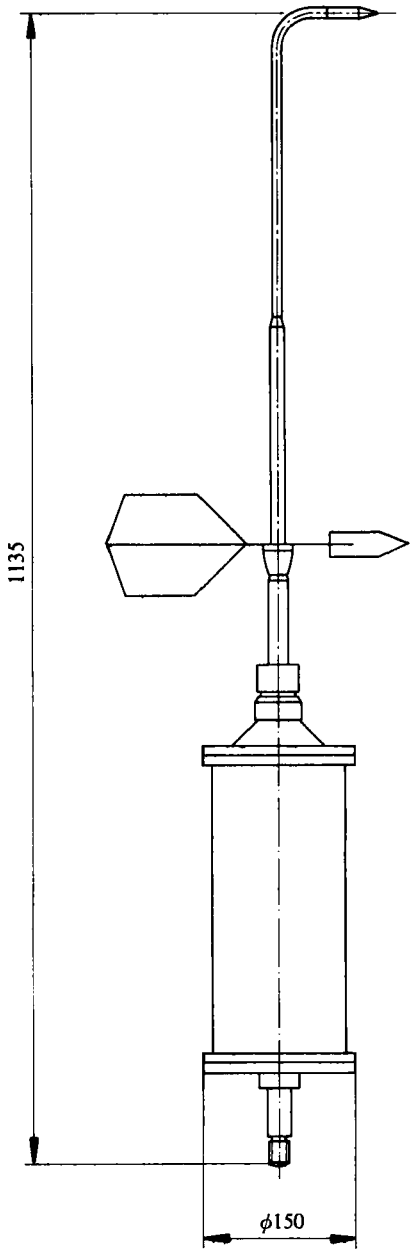

FIGURE 2. Details of the pressure sensor, with the probe at the tip, the connecting pipe, the vane and the fitting to the large lower cylindrical housing, inside which (not shown) is the pressure transducer. The magnetic fluid (not shown) is used to seal the fitting of the turnable pipe.

Usually the agreement for fresh wires would be better, in the order of 2%, and thus we suspect calibration problems when fresh wires showed differences. We simply treat these two errors as an additional source of scatter. This scatter is about 5% for the wave height, which amounts to a 5% error in the pressure transfer function. This error is, however, automatically included in our later error analysis, see also §8.1. We are confident that these problems in the wave measurements are not associated with phase errors.

In 1977 all wave measurements showed an unexpected type of error in a sudden jump of offset. This was not a frequent error (typically once a day) and did not usually interfere with the fluctuation measurements. It did introduce sources of error for the mean surface height which therefore in 1977 was only determined to within ± 8 cm, sufficient for our purposes. No such problems, either in gain or in offset, were noticeable in 1981.

2.3. *Problems particular to the site*

2.3.1. *Exposure*

The site is exposed to swell and well-developed seas, which not only complicates the directional properties of the wave field, but also demands fairly robust equipment as already remarked by Snyder *et al.* (1981) and by Dobson & Elliott (1978). This point was underscored in the 1981-experiment, which was terminated two weeks early after the spars had been twisted in a storm and all instruments on the needle destroyed.

2.3.2. *Wave scattering at the mast*

The waves are reflected at the mast and the correlations between the reflected waves (surface and atmospheric) and the incoming waves introduce errors, see Snyder (1974) and Papadimitrakis *et al.* (1985, 1986). We have obtained estimates of these errors for a potential flow problem which is similar to, but simpler than the real one. The mathematics is straightforward but too lengthy to be included here. (Details can be obtained from the first author.) We give a short summary only. Notation in this section may differ from that used elsewhere in this paper. We treat wave scattering at a cylindrical mast of radius a, which ends at mean water level so that the constant mean wind $U(z) = U(1, 0)$ notices a surface characterized by an incoming wave, a reflected wave and the flat circular area, $r \leqslant a$. Factoring out the factor $e^{-i\omega t}$ we let the incoming wave be, $\boldsymbol{k} = (k_1, k_2)$,

$$\tilde{\zeta} = Z\zeta, \quad \zeta = e^{ikr\cos\Theta}$$

and consider the point of observation at (r, Θ_1). Pressures will be non-dimensionalized by $(kZ)c^2$, waveheights by Z. The pressure due to the incoming wave is

$$p = -\left(\frac{U}{c}\cos\Theta - 1\right)^2 e^{-kz}\zeta. \tag{2.1}$$

For the two asymptotic cases $kr \ll 1$ and $kr \gg 1$ we can show that the corrections are small and closer inspection shows this to be true also for $kr \sim 1$.

For $kr \ll 1$ ($kr < 0.5$) the pressure induced by the scattered wave is

$$p_s(r, \Theta_1) = \left(\frac{a}{r}\right)^2 P(r, \Theta - \Theta_1)\cos(\Theta - \Theta_1) \tag{2.2}$$

where $P(r, \Theta - \Theta_1)$ is a function $O(1)$.

For $kr \gg 1$ ($kr \gtrsim 1.5$) we obtain

$$p_s(r, \Theta_1) = -\left(\frac{U}{c}\cos\Theta_1 - 1\right)^2 e^{-kz}\zeta_r(r, \Theta_1), \tag{2.3}$$

which is, as expected, the same relation between pressure and wave height as (2.1), since ζ_r is the reflected wave

$$\zeta_r = \left(\frac{2\pi}{kri}\right)^{\frac{1}{2}}(1 - 2\cos(\Theta - \Theta_1))(\tfrac{1}{2}ka)^2 e^{ikr}. \tag{2.4}$$

In our experiment $a = 0.30$ m, $r = 2.20$ m and $\Theta_1 \approx \frac{1}{2}\pi$, since the spars were orthogonal to the wind. The corrections can introduce a large error only when the unperturbed pressure is small or with (2.1) and (2.2) and (2.4) only when

$$\left(\frac{U}{c}\cos\Theta - 1\right)^2 < \left(\frac{a}{r}\right)^2 \approx \frac{1}{50}, \tag{2.5}$$

where we have taken into account in (2.4) that $(\frac{1}{2}ka)^2 \lesssim \frac{1}{50}$ for $f \leqslant 0.5$ Hz.

If the true pressure wave transfer function γ – to be introduced in more detail in §4 and shown in figures 7 and 8 – satisfies $|\gamma| < 0.02$ we must expect the measurements to be dominated by errors. However, such a small value of γ at a particular frequency requires an extremely small directional spread of the incoming wave field, which is never encountered. By keeping the spars orthogonal to the wind we avoid the severest perturbations, arising when the scattered waves are propagating against the wind (see (2.3), also Papadimitrakis *et al.* (1985, 1986). We note that directional spread is beneficial in reducing reflection effects, so that these are more serious in the laboratory than in the field.

A further effect of scattering is the non-exponential decay of the scattered amplitude with height when $kr \lesssim 1$ – for the assumed potential flow and mean wind field – but again this perturbation can be shown to be negligible.

The effect of the scattered wave on the phase of the total wave height is negligible in any circumstance at the position of the resistance wires, and at the position of the underwater pressure sensor it is of the order $(ka)\,a/r = 0.18$ (11°) at $f = 0.5$ Hz and correspondingly less at lower frequencies. The resulting error for the directional analysis is negligible.

We explain why we may neglect scattering effects, even though Snyder (1974) could clearly demonstrate the dominance of upwind travelling waves in his pressure measurements. Snyder assumed an effective reflector diameter $a_s = 3$ m and a distance $r_s = 125$ m. We note the following.

(i) The factor $(a/r)^2$ in (2.5) results from near-field estimates ($kr < 0.5$) and in the far field ($kr > 1.5$) should be replaced by $(ka)^2(2\pi/kr)^{\frac{1}{2}}$, which is smaller than $(a/r)^2$ for $f < 0.35$ Hz (and not much larger for $f \approx 0.5$ Hz).

(ii) Snyder's measurements were subject to far-field scattering, and the relevant quotient

$$Q = \left(\frac{a_s}{a}\right)^2\left(\frac{r}{r_s}\right)^{\frac{1}{2}} = \frac{100}{7.5} = 13 \tag{2.6}$$

explains why his scattered waves are larger than ours.

His figure 13 at least qualitatively supports the wavenumber dependence (2.4) of the scattered amplitude.

Only the coherence between the pressure associated with the scattered wave and the incoming wave causes an error. In the far field $kr \gg 1$, a scattered component has usually lost coherence with the incoming field, although details depend on the incoming wave spectrum. Thus scattering did not give rise to any errors in Snyder's (1974) experiment, only to an unusual directional distribution. In our case, where kr is not sufficiently large to destroy coherence, only $\frac{1}{2}ka \ll 1$ allows us to neglect the perturbation. Incidentally, again by (2.6) we expect a dominant scattering contribution from the ships in our experiment. We have explained why this does not cause an error, and our directional distribution is so crudely determined (as discussed in §5) that the scattering contribution is negligible in any case.

2.3.3. *Flow distortions*

The needle is slim and should not at $r = 2$ m introduce any serious flow distortions but the same is not necessarily true for the protruding stump of the mast. However, this should not introduce a serious error for the determination of the transfer function γ, because the pressure represents an integrated effect over a larger area and height. The main effect of flow distortions due to the stump should be similar to an incorrect calibration of the anemometers by a few per cent.

3. Data analysis

3.1. *Standard data treatment*

The environmental data were simply averaged and after simple quality checks stored as half hourly averages. The pressure and wave height data were all analysed by a standard package.

(i) Short intervals of missing data were interpolated.

(ii) The analysis period was selected as $T = 2^{14} \times \frac{1}{10}$ s $= 27.5$ min for 10 Hz series, $T = 2^{12} \times \frac{1}{2}$ s $= 34$ min for 2 Hz series and each stretch of data of length T was multiplied with the cosine-bell-function

$$B(t) = \left(\frac{2}{3}\right)^{\frac{1}{2}} \left(1 - \cos\frac{2\pi t}{T}\right)$$

in order to reduce the effects of drift on the spectra.

(iii) These data were then Fourier-transformed in one block and the resulting high-resolution spectral estimates were box-car averaged to yield band-averages with 32 degrees of freedom. The corresponding bandwidth was $\Delta f = \frac{5}{512}$ Hz for the 10 Hz series and $\Delta f = \frac{1}{128}$ Hz for the 2 Hz series.

All pressure signals originally sampled at 10 Hz were analysed twice, first as 10 Hz series, and then in order to obtain cross-spectra with the wave height from the resistance waves, the data were filtered to a 2 Hz series and analysed further starting at item (ii) above. The spectra obtained from the 2 Hz series formed the material for the more detailed analysis, and in fact the bandwidth was widened to $\frac{5}{128}$ Hz at a later stage in order to speed up the analysis. The high-frequency data were not extensively used but nevertheless proved useful for quality control.

3.2. *Data rejection*

We give separate accounts for (*a*) 1977 and (*b*) 1981.

(*a*) 1977

Roughly 100 h of data were analysed as described in §3.1, yielding about 200 spectral matrices (of dimension $5 \times 5 \times 128$). Of these 200 runs, about 30% were eliminated for one of the following reasons.

(i) During the run a sudden change of offset occurred in one of the wave measurements, see §2.2.3.

(ii) One of the resistance wires became entangled.

(iii) Some of the pressure measurements showed a broad peak at $f \approx 3$ Hz. We are sure that this is an instrumental error but in spite of extensive searching we have not been able to detect where the error arose. In most cases only one of the instruments showed this error.

The error could not be linked to any particular pressure sensor, transducer or position on the needle. In most cases the high-frequency error did not affect the low-

Day	Time	N^a	U^b (m/s)	$f_u{}^c$ (Hz)	$f_p{}^d$ (Hz)	$f_{swell}{}^e$ (Hz)	$\Theta_u{}^f$ (°tr. N)	$\Theta_p{}^g$ (°tr. N)	$\Theta_{swell}{}^h$ (°tr. N)	$H_s{}^j$ (m)	$z_{lower}{}^j$ (m)	Δz^k (m)	PR^l
1977 June													
13	10.25–15.10	1–8	3.8–7.2	0.4–0.22	0.35–0.28	0.14	230–260	210–170	160–120	0.32–0.23	2.80–3.60	2.96	1, 2
13	16.14–17.57	9–12	5.7–6.7	0.27–0.23	0.43	0.15/0.25	260	270–210	150/10	0.25–0.28	1.80–1.90	2.34	9–12
14	10.54–12.02	13–14	4.6–2.9	0.34–0.53	0.34	0.12	220	240	160	0.36–0.34	2.39–2.43	0.26	13
14	16.52	15	5.3	0.30	0.24	0.12	230	170	145	0.27	2.93	0.26	15
14	18.17	16	5.7	0.27	0.23	0.12	235	175	155	0.25	0.85	2.34	16
20	11.15–12.23	17–18	5.4–5.1	0.27–0.30	—	0.11	105–90	—	120	1.46–1.63	3.25–3.00	2.96	—
20	17.06–18.15	19–20	3.4	0.46	—	0.11	50–40	—	90	1.20	2.88	2.96	—
21	12.16–18.08	21–26	1.1–4.6	1.43–0.34	—	0.10/0.14 0.20	30–110	—	110–130	0.80–1.12	2.51–4.00	2.96	—
21	20.20–21.28	27–28	5.5–5.1	0.28–0.31	—	0.10/0.14 0.17	120	—	110	0.82–0.79	1.43–1.62	2.34	—
22	9.14–12.36	29–33	7.0–5.5	0.22–0.28	—	0.14/0.18	130–120	—	130–125	1.12—1.23	4.01–3.60	2.96	—
22	13.44	34	5.7	0.27	—	0.16/0.23	120	—	145	1.05	2.85	2.96	—
23	13.36	35	1.6	0.96	—	0.10/0.18	50	—	90/145	0.60	0.86	2.34	—
23	15.08	36	1.7	0.90	—	0.10/0.19	60	—	100/145	0.63	2.43	0.26	—
23	16.26–17.34	37–38	1.7–2.1	0.90–0.71	—	0.18	90–120	—	145	0.61–0.60	1.68–1.60	0.26	—
29	15.14–19.47	39–46	6.4–8.4	0.24–0.19	0.20–0.24	0.14	125–135	105–70	130	0.56–0.77	4.10–3.48	2.96	—
30	9.22–20.02	47–63	7.0–10.0	0.22–0.15	0.30–0.24	0.18	30–50	70–40	100–150	0.90–1.20	2.51–4.14	2.96	61–63

July													
3	13.09–17.46	64–67	4.1–1.4	0.43–1.37	0.35	0.10	45–90	60	90–130	0.58–0.48	2.37–2.97	2.96	64–67
3	18.57–20.39	68–70	1.1–1.7	1.43–0.92	—	0.18	80–110	—	140	0.37–0.36	1.41–1.79	2.34	68
4	11.45–13.27	71–73	3.8–4.3	0.41–0.36	0.37	0.17	180–150	80–110	120	0.28	2.61–3.10	2.96	71–73
5	9.19	74	5.9	0.26	0.26	0.10	160	195	95–120	0.47	4.16	0.02	74
5	11.31–13.13	75–77	6.2–5.6	0.26	0.26–0.30	0.12	150	170	110–120	0.49–0.53	0.75–1.36	2.34	75–77
6	9.57–13.21	78–82	5.8–4.9	0.27–0.32	0.34–0.26	0.12	180	160	110–150	0.40	1.78–1.84	2.34	78–82
6	19.59	83	3.4	0.46	—	0.19	205	—	145	0.76	3.27	2.96	—
7	10.37–17.15	84–92	5.9–4.2	0.26–0.37	0.25	0.12	160	150	150	0.41–0.43	3.92–2.24	0.26	84–92
8	14.20–15.28	93–94	5.3–4.8	0.29–0.32	—	0.24	170–160	—	165	0.59–0.56	1.19–0.90	2.34	93–94
8	16.36–18.50	95–98	3.9–4.5	0.40–0.34	—	0.23–0.18	190–165	—	160–140	0.56–0.64	2.59–2.66	2.96	95–96
9	9.21	99	8.0	0.20	0.22	—	185	160	—	0.86	3.29	2.96	99
9	10.56–16.03	100–106	4.2–6.8	0.23–0.37	0.18–0.22	—	170–160	160–120	—	0.65–0.76	0.99–1.74	2.34	100–106
10	8.49–10.32	107–109	6.0–5.9	0.26–0.27	0.17–0.19	0.12	130	130	140–105	0.80–0.72	2.96–3.12	2.96	107–109
10	11.27–15.46	110–115	5.6–6.3	0.28–0.25	0.18–0.20	0.12	135–125	140–120	130–110	0.72–0.76	1.10–1.47	2.34	110–112
10	16.56– to	116–134	4.7–7.5	0.33–0.21	—	0.14–0.11	100–135	—	105–140	0.72–1.17	2.65–3.95	2.96	—
11	6.43	—	—	—	—	—	—	—	—	—	—	—	—
1981													
Sept.													
30	10.40–14.30	1–6	11.5–12.0	0.1–0.08	0.17	—	15–5	30±20	—	1.52–1.87	5.60–5.40	—	—
30	15.00–21.00	7–16	9.8–11.5	0.15–0.11	0.13	—	(−10)–10	30±20	—	1.83–1.45	5.60–6.85	—	—
Oct.													
1	9.40–12.30	17–21	9.9–8.4	0.15–0.19	0.16	—	−15–(−10)	40±20	—	1.32–1.21	5.85–5.55	—	—
1	12.50–18.30	22–31	8.7–5.5	0.17–0.28	0.15–0.17	—	−60–(−24)	40±40	—	1.28–0.76	5.38–6.36	—	—
3	8.26–9.30	32–33	11.0–12.2	0.12–0.08	0.16	—	30	10±10	—	2.00–1.74	6.04–5.92	—	—
3	12.20–19.03	34–45	9.5–12.2	0.16–0.08	0.16–0.15	—	20–5	60±30	—	1.15–1.64	6.05–5.42	—	—

All frequencies in Hz. All directions in degrees (N = 0, E = 90) towards which wind or waves are proceeding. Ranges given usually very roughly indicate a development in time, but in particular for wave directions may also indicate scatter.

[a] Run number. [b] Wind speed. [c] Frequency at which $U = c$. [d] Peak frequency of wind-sea, if definable. [e] Prominent swell frequencies. [f] Wind direction (toward). [g] Wave direction at $f = f_p$. [h] Wave directions at $f = f_{swell}$. [i] $H_s = 4\langle\zeta^2\rangle^{\frac{1}{2}}$, sign. wave height. [j] Height of lower pressure sensor over *mwl*. [k] Vertical separation of pressure sensors. [l] Runs with simultaneous *PR* buoy measurements.

TABLE 1. Run summary

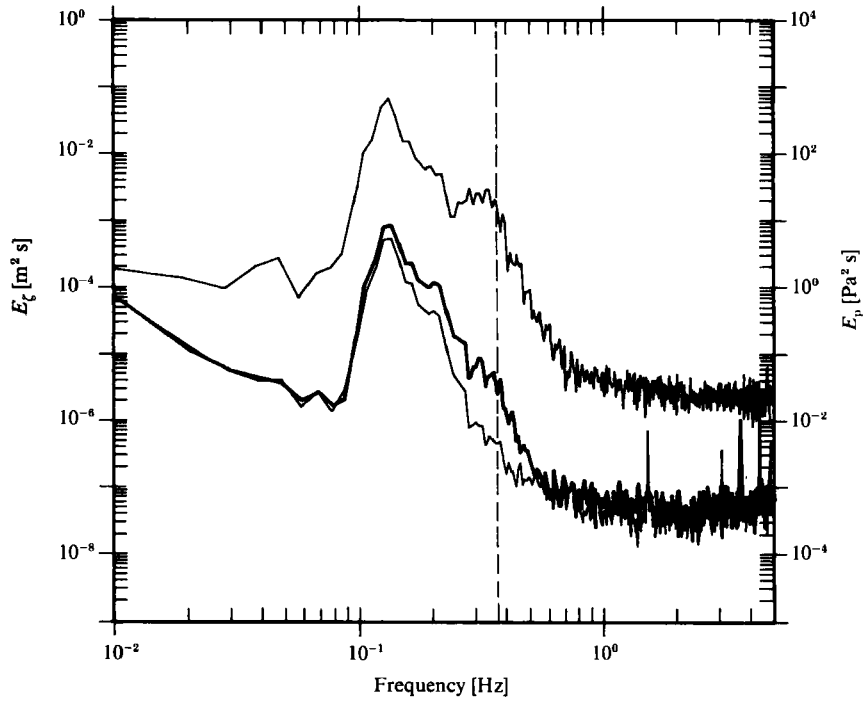

FIGURE 3. Pressure spectra for run 1, on 77/13/6 10.25. The upper line shows the underwater pressure, hydrostatically converted to wave height, the two lower ones the atmospheric pressure, the thicker line from the lower sensor.

frequency ($f \leqslant 0.5$ Hz) signal, as could be checked by comparison with the other sensor and by the high coherence between pressure and waves.

In some cases the high-frequency peak was extremely large and broad and there was substantial evidence (very peculiar spectral shapes, low coherence with the waves) that the low-frequency parts of the spectrum were unreliable. Such cases were rejected.

(iv) During one run (of about 4 h duration, on July 1, not included in table 1) with high wind velocity ($U \approx 11$ m/s) the lower pressure probe had been wetted by a wave. Although this was visually observed only at the end of the run, when the rubber dinghy was approaching the needle, we discarded all of the data obtained on this high wind speed run. The spectra were extremely strange (in our opinion obviously distorted); the spectra obtained from the upper probe were also very peculiar. While we have no reliable explanation for the strange results obtained from the upper probe (perhaps port blockage due to spray), we considered these data too suspect for further analysis. (The protocol at the monitoring station had also noted very unusual pressure signals for this run.)

(v) Some runs were test runs in which we had chosen some particular geometry; if this geometry was not well suited for the standard analysis such runs were excluded from the data set.

(*b*) 1981

We analysed 23 h of data according to §3.1 and none of the runs was rejected. All high-frequency pressure spectra showed an unexplained peak at $f \approx 4.5$ Hz, which was typically smaller than those seen in 1977. The coherence between waves and

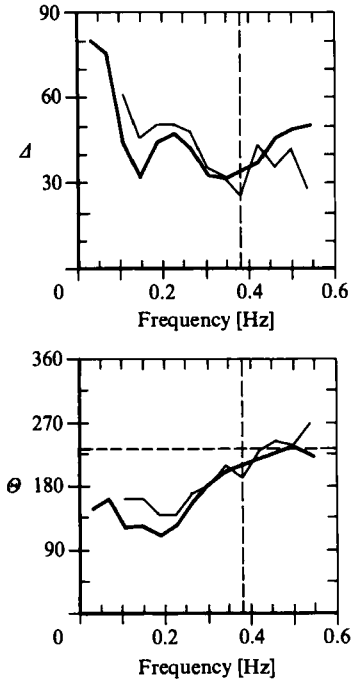

FIGURE 4. The directional spectrum for the same run as in figure 3. The heavy line is obtained from pitch and roll information, the thin line from array information. Θ_m is the mean direction, Δ the r.m.s. width, $\Delta = (2/(s+1))^{\frac{1}{2}}$ (5.2). The dashed lines show direction Θ_u into which the wind is blowing and the frequency at which $U_5 = c$.

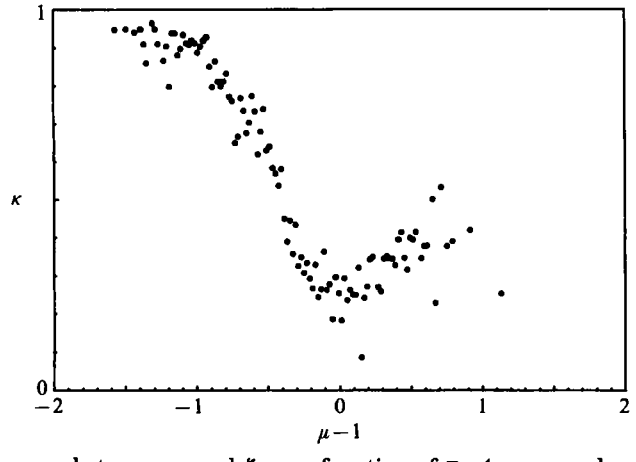

FIGURE 5. Coherence κ between p_1 and ζ_1 as a function of $\bar{\mu}-1$, averaged over all runs, with 200 slots on the μ-axis and a straightforward unweighted average over the coherences. The minimum in the coherence at $\mu = 1$ is due to the minimum of α and β shown in figures 7 and 8.

pressure was high at low frequencies and we saw no reason to assume that the unexplained high-frequency peak had influenced the low-frequency data.

3.3. *The data set*

The data set consisting of all runs accepted for further analysis comprises 134 runs from the 1977 experiment and 45 runs from 1981, with each run contributing a spectral matrix ($128 \times 5 \times 5$ in 1977, $128 \times 3 \times 3$ in 1981). The selected runs with some

of their pertinent features are listed in table 1. In the summer experiment of 1977 most of the wave spectra had a large or even dominant swell component and in many cases the spectra were such a mix of swell and wind-sea that a clear division between wind-sea and swell was difficult. It is not surprising that in such circumstances the spectra were not even remotely similar to a JONSWAP spectrum (Hasselmann *et al.* 1973).

In 1981 the windspeed was higher and a JONSWAP-like wind-sea was usually observed, but even in these cases a swell component coming from the northwest was normally present, although not usually discernible as a peak in the frequency spectrum.

There was always a strong wave-induced component in the pressure spectra and in particular over swell the spectra would rise by a factor of about 500 over a somehow extrapolated background level. In such cases a typical value of the (square root) coherence between (swell) waves and pressure would be $\kappa \approx 0.9$, which would drop to $\kappa \approx 0.5$ above wind-sea. These points are illustrated in figures 3, 4, 5.

4. Preliminaries for further analysis

We introduce the notation p_1, p_2 for the pressure measured by the lower and upper sensor and $\zeta_1, \zeta_2, \zeta_3$, for the wave height obtained from the two resistance wires and the underwater pressure sensor; here ζ_1 is the sensor under the air pressure sensor. For the 1981 experiment we have only p_1, ζ_1 and ζ_2.

Let $a(\boldsymbol{k}, \omega)$ and $b(\boldsymbol{k}, \omega, z)$ be the Fourier transforms of $\zeta(\boldsymbol{x}, t)$ and $p(\boldsymbol{x}, z, t)$; we then introduce the non-dimensional transfer function $\gamma = \alpha + \mathrm{i}\beta$ as

$$b^{\mathrm{w}}(\boldsymbol{k}, \omega, z) = \rho_{\mathrm{a}} c^2 k \gamma a(\boldsymbol{k}, \omega), \tag{4.1a}$$

$$b = b^{\mathrm{w}} + b^{\mathrm{t}}, \quad \langle b^{\mathrm{t}} a^* \rangle = 0, \tag{4.1b}$$

where $c = \omega/k$, $k = |\boldsymbol{k}|$ and b^{w}, b^{t} are the wave-induced and turbulent pressure components. Here $\gamma = \alpha + \mathrm{i}\beta$ is a function of non-dimensional parameters of which we shall consider only μ and λ

$$\mu = \boldsymbol{k} U_5 \frac{1}{\omega} = \frac{U_5}{c} \cos\Theta; \quad \lambda = kz. \tag{4.2}$$

For convenience in later comparisons: our β induces a growth rate

$$\frac{\mathrm{d}E(\omega)}{\mathrm{d}t} = \frac{\rho_{\mathrm{a}}}{\rho} \omega \beta E(\omega). \tag{4.3}$$

We shall use the notation $a(\boldsymbol{k}, t)$ and $a(\boldsymbol{x}, \omega)$ as

$$a(\boldsymbol{k}, t) = \int a(\boldsymbol{k}, \omega) \, \mathrm{e}^{-\mathrm{i}\omega t} \, \mathrm{d}\omega,$$

$$a(\boldsymbol{x}, \omega) = \int a(\boldsymbol{k}, \omega) \, \mathrm{e}^{\mathrm{i}\boldsymbol{k}\boldsymbol{x}} \, \mathrm{d}\boldsymbol{k}_1 \mathrm{d}\boldsymbol{k}_2$$

and likewise for $b(\boldsymbol{k}, z, t)$, $b(\boldsymbol{x}, z, \omega)$. Similarly $a_1(\omega)$ is the Fourier-component of $\zeta_1(t)$, $b_1(\omega)$ that of $p_1(t)$ etc. We have used the velocity scale U_5 in μ for the same reasons as Snyder *et al.* (1981), but shall discuss other choices in §7. In (4.2) all velocities and frequencies are understood in the system in which the mean surface current v vanishes. In (4.1) we may replace $c^2 k$ by g when considering deep-water waves but

generally we prefer (4.1), because the acceleration of gravity does not appear in the equations for the atmospheric response (Miles 1957), unless we include stability effects (Janssen & Komen 1985; Makin 1983*b*). Perhaps (4.1) also holds for shallow-water waves with the same γ as for deep water. This extension should be appropriate if the orbital motion tangential to the surface is not very important for the pressure response, as one might expect if the mechanism is mainly inviscid.

Our principal source of information is the data set consisting of the cross-spectral matrices

$$C_{ij}(w) = \frac{1}{\Delta\omega}\langle d_i d_j^* \rangle; \quad i,j = 1,\ldots,5, \tag{4.4}$$

where $\langle\,\rangle$ generally denotes averaging (in the present connection bandwidth averaging) and

$$d_i = b_i(\omega, z) \quad \text{for } i = 1,2; \quad d_i = a_i(\omega) \quad \text{for } i = 3,\ldots,5.$$

Our aim is to deduce the form of $\gamma(\mu,\lambda)$, to which end we must:

(i) model the directional distribution of the wave field in order to estimate μ;

(ii) estimate the λ-dependence of $\gamma(\mu,\lambda)$ in order to extrapolate to $\lambda = 0$, and

(iii) finally estimate the μ-dependence of

$$\gamma(\mu, \lambda = 0) = \alpha(\mu, 0) + \mathrm{i}\beta(\mu, 0).$$

This detailed analysis was not performed on the high-resolution data set, since in each analysis step many additional results were added to the data set and the data handling threatened to become clumsy and unmanageable. As we do not believe that very much can be gained from the high resolution $\delta f = \frac{1}{128}$ Hz we have widened the analysis bandwidth to $\Delta f = 5\delta f$. We further limited the analysis to frequencies $f \leqslant \frac{69}{128}$ Hz, because owing to the rapid loss of coherence with λ very little if any information on γ is contained at higher frequencies. Finally, the directional analysis showed that for frequencies $f < \frac{14}{128}$ Hz the directional distribution became unreliable. Thus finally in step (iii) only 12 frequency bands were used $f_n = (9+5n).128$ Hz, $n = 1,\ldots,12$, each band with 160 degrees of freedom.

Our analysis does not exactly follow that of Snyder *et al.* (1981), but is certainly very similar.

5. Directional wave spectra

The linear array consists of two resistance wires 4 m apart and in 1977 we also had the pressure sensor nearly halfway between the two. In 1981 we had one lag $L_1 \approx 4$ m and in 1977 we had in addition two nearly identical lags $L_2 \approx L_3 \approx 2$ m, and the difference $|L_2 - L_3|$ depended slightly on the orientation of the spars but was always less than 0.50 m.

Thus in 1977 we had six data points at each frequency to determine the directional spectrum, namely the three cross-spectra

$$A_{ij}(w) = \langle a_i a_j^* \rangle \frac{1}{\Delta\omega} \quad (i,j = 1,\ldots,3; i \neq j), \tag{5.1}$$

while in 1981 only two data points were available. Thus in 1981 only two directional parameters could be determined, and in view of the small distances L_i and the near redundancy between the cross-spectra belonging to the lags L_2 and L_3 we decided to determine only two directional parameters for the 1977 data set.

We model the directional distribution $S(\Theta,f)$ – which for brevity we often denote by $S(\Theta)$ – by the mean direction Θ_m and sharpness parameter s using the function

$$S(\Theta) = \frac{1}{N(s)} \cos^{2s} \tfrac{1}{2}(\Theta - \Theta_m), \tag{5.2}$$

where $N(s)$ is a normalizing factor, to ensure

$$\int S(\Theta)\, d\Theta = 1$$

and the two-dimensional wave spectrum $E(f,\Theta)$ is given by ($\omega = 2\pi f$)

$$E(f,\Theta) = E(f)\, S(\Theta) \tag{5.3}$$

(Longuet-Higgins, Cartwright & Smith 1963; Mitsuyasu *et al.* 1975; Hasselmann, Dunckel & Ewing 1980; Donelan, Hamilton & Hui 1985). The directional data were first normalized to

$$D_\alpha = \frac{A_{ij}}{(A_{ii} A_{jj})^{\frac{1}{2}}}, \tag{5.4}$$

with $\alpha = 1, \ldots, 3$ denoting the combinations (i,j) in (5.1) for 1977 and $\alpha = 1$ in 1981. The model values $\hat{D}_\alpha$ can then be calculated for any parameters (Θ_m, s) in (5.2) and the best fit is chosen by minimizing

$$\epsilon^2 = \epsilon_\alpha W_{\alpha\beta} \epsilon_\beta^* \quad (\alpha, \beta = \pm 1, \ldots, \pm 3), \tag{5.5}$$

with

$$\epsilon_\alpha = \hat{D}_\alpha - D_\alpha,$$

$$\epsilon_{-\alpha} = \epsilon_\alpha^*,$$

where $W_{\alpha\beta}$ is the inverse of the covariance matrix $V_{\alpha\beta}$

$$V_{\alpha\beta} = \mathrm{cov}\,(D_\alpha D_\beta^*) \quad (\alpha, \beta = \pm 1, \ldots, \pm 3), \tag{5.6}$$

with $D_{-\alpha} = D_\alpha^*$. For a Gaussian process $V_{\alpha\beta}$ is known (see for instance, Müller, Olbers & Willebrand 1978). For the 1981 data the choice of weight matrix did not influence the results since we had two parameters and two data points. For the 1977 data the fits were not always consistent, lack of fit occurring mainly at low frequencies $f < 0.25$ Hz. We considered a fit consistent if $\epsilon^2 < \chi^2$ $(\nu, Q = 0.05)$ or since $\nu = 4$, $\epsilon^2 < 9.5$, in the notation of Abramowitz & Stegun (1965). We did not take these statistical tests very seriously, since they are based on the approximation that the D_α have a close to normal distribution, which fails when the coherences $|D_\alpha|$ are close to unity, as is the case at low frequencies when $kL \ll 1$. In both experiments the array was essentially linear so that only

$$\tilde{\Delta} = |\Theta_m - \Theta_a|,$$

where Θ_a is the array angle can be resolved, which leaves us with two solutions $\Theta_{1,2} = \pm\tilde{\Delta} + \Theta_a$. Additional criteria were applied to select the proper solution.

In the wind-sea region ($U > c$) we chose the solution which gave the best agreement between wind and wave direction. In the swell domain we have distinguished three cases.

(i) Both directions indicate swell running towards the coast. A further criterion must be invoked which is explained in §7 and involves the cross-spectrum between pressure and wave height.

(ii) One direction only corresponds to swell running onto shore, this is the proper direction.

(iii) Both directions correspond to offshore swell and are thus unacceptable. The analysis was flagged a failure.

Another failure, which occurred only for the 1981 data, were 'array-locked' solutions, in which Θ_m agreed to within one degree with $\Theta_a = 108°$. At low frequencies $f = \frac{9}{128}$Hz and $f = \frac{14}{128}$Hz this happened in nearly two thirds of all cases, and in 15 cases also occurred at higher frequencies. Although $\Theta_m = \Theta_a$ is a reasonable swell direction, corresponding to swell from about Scotland, we decided to discard these solutions.

Eventually we discarded the directional results for $f < \frac{14}{128}$Hz, since for the 1977 data the resulting directions varied strongly from run to run and for 1981 array locking was too frequent.

The directional results were surprisingly good for the 1977 experiment and, probably owing to the presence of the two additional lags L_2 and L_3 in 1977, better than those obtained in the 1981 experiment. In figure 4 we show typical comparisons of the results obtained from array data and buoy data. Plots of the average differences between the mean propagation directions obtained from the two data sets show no significant bias (not shown).

The differences between pitch and roll results and those from the array are not due entirely to sampling error. The standard deviation of individual differences is $\sigma_\Delta \approx 30°$ (not shown), whereas for the difference ΔPR between two independent pitch and roll measurements, we expect only

$$\Delta PR = \sqrt{2}\sigma_2 \approx \sqrt{2}/\nu^{\frac{1}{2}} = 7°$$

for $\nu = 160$ degrees of freedom (Long 1980*a*; Hasselmann *et al.* 1980). Scanning through all directional plots with simultaneous PR and array information (an example is shown in figure 4 and in Hasselmann *et al.* 1986) we estimate the standard error σ_1 of the mean direction obtained from array data to be less than $3\sigma_2$, whereas $\sigma_1 \approx 6\sigma_2$ is required to explain σ_Δ. We conclude that additional systematic errors occur, and, in fact, these are fairly evident in the directional plots.

There are various sources for such systematic errors, be they instrumental, due to the algorithms, or to the time difference between buoy and array measurements. However, we can neither trace back to the origin of these errors, nor are they repeatable from day to day, and therefore we cannot correct for them. To judge by the scatter of the real part of the pressure transfer function, which is discussed in more detail below in §7.5 the array data alone are not to blame for the systematic errors, and it appears that the error is fairly equally divided between both systems, except at low frequencies $f < \frac{14}{128}$ Hz.

6. The vertical dependence

We have estimated the vertical dependence only for the 1977 experiment in which pressure was measured at two levels simultaneously, whereas only one level was occupied in 1981. The vertical dependence deduced from the 1977 data was used to extrapolate the 1981 data to the surface.

The data base for our analysis of the λ-dependence of $\gamma(\mu, \lambda)$ consisted of the six cross-spectra

$$B_{ij} = \langle b_i a_j^* \rangle \frac{1}{\Delta\omega} \quad (i = 1, 2, \quad j = 1, 2, 3), \tag{6.1}$$

where b_i and a_j are the transforms of p and ζ as defined in §4. Our aim is to estimate

$$\Gamma(\mu, \lambda) = \gamma(\mu, \lambda)/\gamma(\mu, 0). \tag{6.2}$$

Our analysis was guided by the following considerations:

(i) From other experiments, Snyder *et al.* (1981), Snyder (1974) and Elliott (1972), we anticipated an essentially exponential decay, $\Gamma \approx e^{-\lambda}$, and furthermore only a weak dependence of Γ on μ.

(ii) We wished to decouple the analysis of $\Gamma(\mu, \lambda)$ from the analysis of the surface values $\gamma(\mu, 0)$. In particular we did not want the directional analysis to interfere with the vertical analysis.

Our approach was to obtain estimates r of the ratio r'

$$r'(\lambda_1, \lambda_2) = \frac{\gamma(\mu, \lambda_2)}{\gamma(\mu, \lambda_1)}, \tag{6.3}$$

by minimizing for each run and frequency

$$\epsilon^2 = d_\alpha^* W_{\alpha\beta} d_\beta \quad (\alpha, \beta = \pm 1, \ldots, \pm 3), \tag{6.4a}$$

with

$$d_\alpha = B_{2\alpha} - r B_{1\alpha}, \quad (\alpha = 1, \ldots, 3, \quad d_{-\alpha} = d_\alpha^*), \tag{6.4b}$$

$$W_{\alpha\beta} = (V^{-1})_{\alpha\beta}, \quad V_{\alpha\beta} = \mathrm{var}\,(d_\alpha d_\beta^*). \tag{6.4c}$$

This analysis includes the information from all three wave measurements with the appropriate weighting. We have chosen this method because by modelling ratios the vertical analysis is decoupled from the directional analysis, in contrast to the refined method of Snyder *et al.* (1981). Our method is much closer in spirit to their simplified analysis, but we hoped to avoid their bias problem. This arises because Snyder *et al.* use estimates $|r_\alpha| = |B_{2\alpha}/B_{1\alpha}|$, which are biased high for each α, whenever the coherences between waves and pressure are low. They circumvent this bias by eliminating low coherences from their sample.

Our approach does have drawbacks. First, unles $\Gamma(\mu, \lambda)$ in (6.2) is close to exponential, information on ratios $r(\mu, \lambda)$ does not easily allow reconstruction of $\Gamma(\mu, \lambda)$.

Second, unlike Snyder *et al.*, we make no use of the information contained in the matrix

$$P_{ij} = \langle b_i b_j^* \rangle(\omega) \quad (i, j = 1, 2)$$

of the pressure–pressure cross-spectra. However, this latter drawback is not severe. Since not only a description of wave induced, but also that of turbulent pressures would be required in the modelling of P_{ij}, only the side conditions

$$P_{11} \geqslant \tilde{P}_{11}, \quad P_{22} \geqslant \tilde{P}_{22} \tag{6.5}$$

would actually yield additional information for $\Gamma(\mu, \lambda)$, where the $\tilde{P}_{ij}$ are the modelled power spectra of wave-induced pressure,

$$\tilde{P}_{ii}(f) = \int |\gamma(\mu, \lambda)|^2 E(f)\, S(f, \Theta)\, \mathrm{d}\Theta, \tag{6.6}$$

and $E(f)S(f, \Theta)$ is the directional wave spectrum (5.3). Since we expect $\Gamma(\mu, \lambda) = \gamma(\mu, \lambda)/\gamma(\mu, 0)$ to be only weakly dependent on μ we also expect (6.5) to introduce only a little new information on the vertical dependence in addition to (6.4). Restrictions on the models arising from (6.5) primarily concern the product $\gamma(\mu, 0)S(f, \Theta)$.

After the analysis (6.4) we have roughly 12×140 estimates of $r(\lambda_1, \lambda_2)$ with corresponding error bars. To test our simplest assumption, that $r(\lambda_1, \lambda_2)$ is only a function of $\Delta\lambda = \lambda_2 - \lambda_1$, which implies, for fixed μ,

$$r(\lambda_1, \lambda_2) = e^{-l(\mu)\Delta\lambda}, \tag{6.7}$$

we have stratified the values of r by $\Delta\lambda$ and taken averages (weighted by the variance σ_r^2 of r) at each $\Delta\lambda$. The results do not differ significantly from those shown in the preliminary report (Hasselmann *et al.* 1986) and are not shown. Briefly we summarize that the departure from

$$r(\Delta\lambda) = \mathrm{e}^{-\Delta\lambda} \tag{6.8}$$

is hardly detectable on a linear scale, but on a logarithmic scale the decay parameter $l(\mu)$ can be seen to decrease for larger values of $\Delta\lambda$, $\Delta\lambda \gtrsim 1.3$.

The imaginary part r_2 of $r(\mu; \lambda_1, \lambda_2) = r_1 + ir_2$ is consistent with zero.

The real part r_1 is positive in all cases considered and we made further checks on

$$l = -\frac{1}{(\lambda_2 - \lambda_1)} \log r_1. \tag{6.9}$$

In the preliminary report we suspected the decrease of l with increasing $\Delta\lambda$ to be due to a bias associated with a low coherence between the pressure p_1 at the lower height and wave height ζ_1. However, although a slight dependence of l on the coherence can be detected (not shown), this cannot explain the decrease of l with $\Delta\lambda$.

In figure 6 we plot l against $\bar{\mu} = U\overline{\cos\Theta}/c$, the bar indicating averaging over directions, and against $\lambda_m = 0.5(\lambda_1 + \lambda_2)$. Each point is a bin average, weighted with the inverse variance of l and each abscissa contains 200 bins. There seems to be an obvious dependence of l on these parameters. Nevertheless, we opt for the very simple description $l = +1$ for the following reasons.

(*a*) The prediction from theory that the wave coherent pressure should decay as $\mathrm{e}^{-\lambda}$ for $\lambda \gg 1$ is very robust. The exponential decay is not generally expected for smaller values of λ, see for instance Townsend (1980) or Long (1980*b*), but $\lambda < 1$ is accessible in this experiment only in conjunction with $\mu < 1$ and there we expect and find roughly exponential decay. The observed departures from exponential decay do not support any theory we know of, and to us some experimental problem still seems to be the most likely explanation, see also (*b*)–(*d*) below.

From the laboratory measurements of Papadimitrakis *et al.* (1986, 1988) there is some evidence for a particular height $\lambda_{hp} \approx 0.2$ below which the pressure remains constant or even increases with height. It is not obvious, how this behaviour found at $f = 1$ Hz, $U/c \approx 2.5$ and in the presence of reflected waves, should be generalized to larger wavelengths, for which (in a non-dimensional framework) our measurements do not indicate such behaviour, as can be seen from figure 6. Townsend's (1980) theory might serve as a guide, but its results are in conflict with our measurements, see §8.2. If we nevertheless assume the existence of a universal $\lambda_{hp} \approx 0.2$, our extrapolation (6.15) of the pressure to the surface will yield values which are too high by 20%. Thus, if necessary, such a correction could easily be applied, but at present we see no necessity for it.

(*b*) No attempt to describe l as

$$l = (h(\mu, \lambda_2) - h(\mu, \lambda_1))/(\lambda_2 - \lambda_1) \tag{6.10}$$

corresponding to

$$\gamma(\mu, 0) = \gamma(\mu, 0) \exp\{-h(\mu, \lambda)\} \tag{6.11}$$

was successful, if the side condition arising from (*a*) $h((\mu, \lambda) \to \lambda$ for $\lambda \to \infty$ was enforced.

(*c*) For large values of λ_1 and $\Delta\lambda$, say $\lambda_1 > 4$ and $\Delta\lambda > 4$, r_1 levels off to a constant value $r_1 \approx 0.1$. This cannot be due to anything other than a bias of our procedure (6.4), the reasons for which we have not looked into in any detail.

(*d*) The correlations of l with μ and λ_m occur in a region

$$\Delta\lambda \geqslant 2, \quad \mu \geqslant 1, \quad \lambda_1 \geqslant 1.5$$

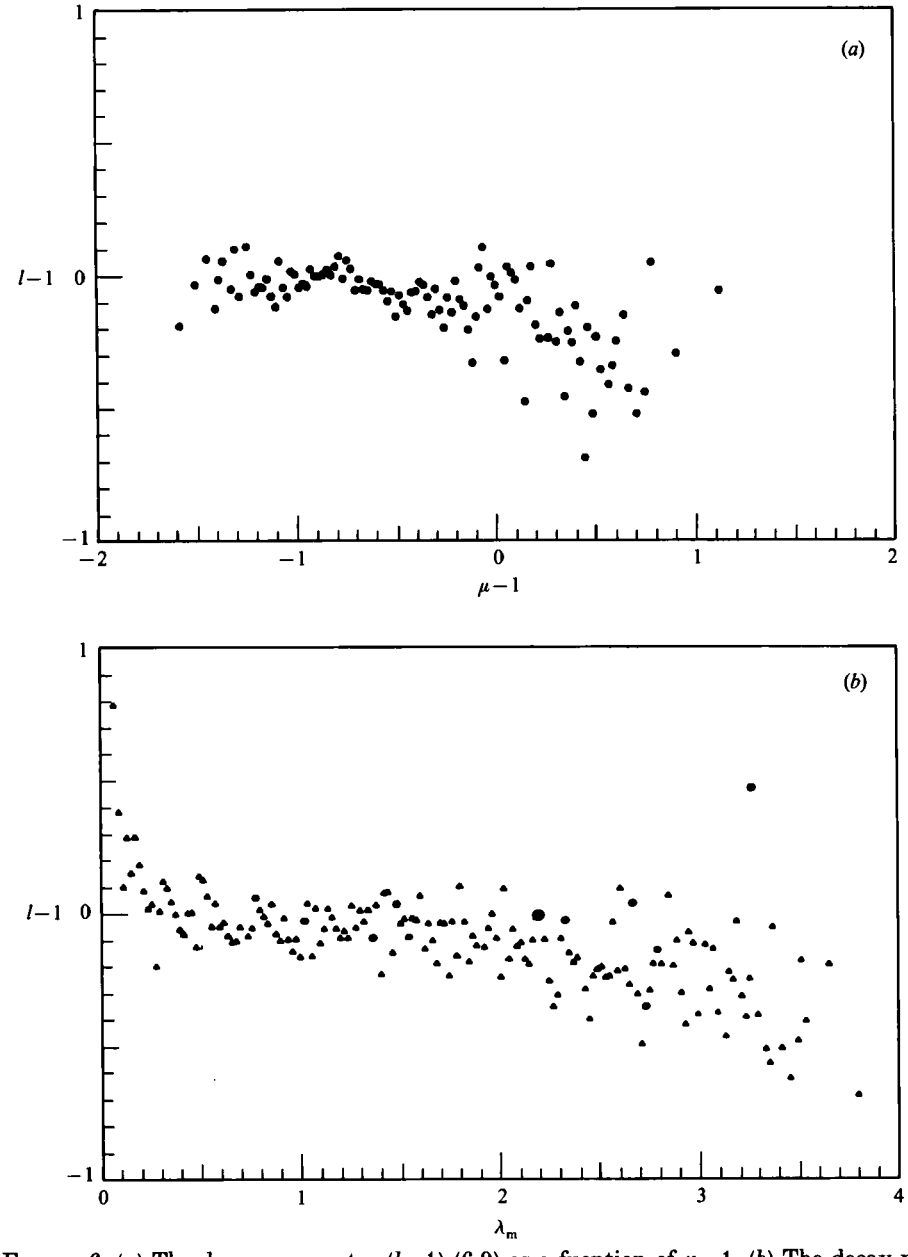

FIGURE 6. (*a*) The decay parameter $(l-1)$ (6.9) as a fucntion of $\mu-1$. (*b*) The decay parameter $l-1$ as a function of $\lambda_m = 0.5(\lambda_1+\lambda_2)$.

where (owing to the dominating wave-number dependence) $\Delta\lambda$, μ and λ_m are all highly correlated, so that the results of correlating l against μ and λ_m are susceptible to the errors mentioned in (*c*).

In our extrapolation to the surface, the influence of the lower probe dominates, as is explained below, and furthermore we have excluded data with $\lambda_1 > 2.3$. If we disregard (*b*)–(*d*) we can, from figure 6(*a*), approximately describe l as

$$dl = l-1 = -0.3(\mu-1) \quad \text{for } \mu > 1$$
$$\delta l = l-1 = 0 \quad \text{otherwise.} \tag{6.12}$$

If we further assume a typical value for the extrapolation distance for $\mu > 1$ to be $\lambda_1 \approx 1.5$, we estimate the average correction factor to be

$$\delta r = \exp(-0.3 \cdot 1.5) = 0.6. \tag{6.13}$$

Thus if we use (6.12) instead of $l = 1$ our values of γ for $\mu > 1$ will be reduced and on average γ will be reduced by a factor of about 0.6.

The estimates $\hat{\gamma}(\gamma_i)$ of $\gamma(\mu, \lambda_i)$ are obtained as

$$\hat{\alpha}(\lambda_i) + i\hat{\beta}(\lambda_i) = \hat{\gamma}(\lambda_i) = \frac{B_{i1}(\omega)}{A_{11}(\omega)} \frac{1}{\rho_a c^2 k} \tag{6.14}$$

with A, B given in (5.1), (6.1). Extrapolation to $\lambda_i = 0$ yields the surface values as

$$\hat{\alpha}_i(0) + i\hat{\beta}_i(0) = \hat{\gamma}_i(0) = \exp(\lambda_i)\hat{\gamma}(\lambda_i) \quad (i = 1, 2). \tag{6.15}$$

Furthermore, the variances $\sigma_\alpha^2(\lambda_i)$ of $\hat{\alpha}(\lambda_i)$ can be estimated and thus the standard deviations $\sigma_{\alpha,i}^2$ and $\sigma_{\beta,i}^2$ of $\hat{\alpha}_i$ and $\hat{\beta}_i$, where according to (6.15)

$$\sigma_{\alpha,i}^2 = \exp(2\lambda_i)\sigma_\alpha^2(\lambda_i). \tag{6.16}$$

For each run and at each frequency the final products of the extrapolation are the weighted means α and β of the $\hat{\alpha}_i$ and $\hat{\beta}_i$ and their standard deviations.

Thus, writing σ_i for $\sigma_{\alpha,i}$

$$\hat{\alpha} = \left(\frac{\hat{\alpha}_1}{\sigma_1^2} + \frac{\hat{\alpha}_2}{\sigma_2^2}\right)\left(\frac{1}{\sigma_1^2} + \frac{1}{\sigma_2^2}\right)^{-1} \tag{6.17}$$

and

$$\hat{\sigma}_\alpha^2 = \left(\frac{1}{\sigma_1^2} + \frac{1}{\sigma_2^2}\right)^{-1} \tag{6.18a}$$

provided the $\hat{\alpha}_i$ and σ_i^2 are consistent with a common mean (at 95 % confidence level), otherwise

$$\hat{\sigma}_\alpha^2 = \left\{\frac{(\hat{\alpha} - \hat{\alpha}_1)^2}{\sigma_1^2} + \frac{(\hat{\alpha} - \hat{\alpha}_2)^2}{\sigma_2^2}\right\}\left(\frac{1}{\sigma_1^2} + \frac{1}{\sigma_2^2}\right)^{-1}, \tag{6.18b}$$

which is equivalent to multiplying the σ_i^2 in (6.17) and (6.18a) by a common factor to enforce consistency of $\hat{\alpha}_1$ and $\hat{\alpha}_2$. The corresponding procedure is applied for $\hat{\beta}$ and $\hat{\sigma}_\beta$. The $\hat{\alpha}$ and $\hat{\beta}$ are thus weighted averages and we note that the influence of the lower pressure probe dominates, first, because of the exponential factor in (6.16) and, secondly, because $\sigma_\alpha^2(\lambda_1) < \sigma_\alpha^2(\lambda_2)$ owing to the decrease of coherence between waves and pressure with height.

For the 1981 data we simply have

$$\hat{\sigma}_\alpha^2 = \sigma_\alpha^2(\lambda_1)\exp(2\lambda_1), \quad \hat{\alpha} = \alpha(\lambda_1)\exp(\lambda_1), \tag{6.19}$$

and likewise for $\hat{\beta}$.

7. The procedure for the analysis of surface values

In this chapter we describe the surface data and the methods used to analyse these. We also describe how we have tested the influences of the directional distribution, currents and assumed displacements of the resistance wires.

7.1. *Data*

The extrapolation to the surface yields roughly 2000 values of $\hat{\alpha}$ and $\hat{\beta}$, comprising the data of 180 runs and 12 frequency bands. For each data point we also have estimates of $\hat{\sigma}_\alpha^2$, $\hat{\sigma}_\beta^2$, of the directional distribution $S(\Theta)$ and the mean windspeed U_5

and direction Θ_u. Except to determine the vertical decay, we have made no use of the horizontally lagged spectra (lags L_1 and L_2) between pressure and wave height. Processing this information would have required an elaborate directional analysis of the product,

$$T(\Theta) = \exp[ikL\cos(\Theta-\theta)]\,\gamma(\mu(\Theta))\,S(\Theta), \tag{7.1}$$

where θ is the array direction. This was not considered worthwhile, since we would gain little information on $\beta(\mu)$.

7.2. *Models*

We try to describe the data by a transfer function depending only on

$$\mu = \frac{U_{\mathrm{m}}}{c}\cos\Theta, \tag{7.2}$$

where U_{m} is a scale for the mean wind speed. We thus try to find a fit of $\hat{\gamma}(\mu,0) = \hat{\alpha}+\mathrm{i}\hat{\beta}$ such that

$$\left.\begin{aligned}\hat{\alpha} &= a_0+a_1A(\mu)+\epsilon_\alpha,\\ \hat{\beta} &= b_0+b_1B(\mu)+\epsilon_\beta,\end{aligned}\right\} \tag{7.3}$$

where the two functions $A(\mu)$ and $B(\mu)$ together with U_{m} characterize the parameterization. The regression constants a_0, a_1, b_0, b_1 are to be determined and ϵ_α, ϵ_β stand for the unexplained, uncorrelated components of the data.

We have tested four models, of which the first three differ only in the choice of the scale U_{m} in (7.2), but have the same functions $A(\mu)$ and $B(\mu)$, while the fourth model attempts to match the parameterization of Plant (1982). Since we cannot by the data discriminate between the quality of the models – as illustrated in figure 7 and discussed in more detail below – we concentrate here on model 1 and for details of the other models refer to Appendix B. Model 1 is given by

$$\left.\begin{aligned}A(\mu) &= -(\mu-1)^2 \quad \text{for } \mu \leqslant 1,\\ A(\mu) &= -0.65(\mu-1)^2 \quad \text{for } \mu \geqslant 1,\end{aligned}\right\} \tag{7.4}$$

and

$$\left.\begin{aligned}B(\mu) &= 0 \quad \text{for } \mu \leqslant 1,\\ B(\mu) &= \mu-1 \quad \text{for } \mu \geqslant 1, \quad \mu = \frac{U_5}{c}\cos\Theta,\end{aligned}\right\} \tag{7.5}$$

and for $a_0 = b_0 = 0$, $a_1 = 1$, $b_1 = 0.2$–0.3 is a good fit to the data of Snyder *et al.* (1981, see their figure 22).

The discussion in §§7.3–7.5 applies for all models.

7.3. *Presentation*

A plot of the data in the form $\hat{\alpha}, \hat{\beta}$ *vs.* μ is helpful for determining A and B, but not as straightforward as may appear at first sight, since only directionally averaged values of μ are available. Thus we plot $\hat{\alpha}$ *vs.* μ_A and $\hat{\beta}$ *vs.* μ_B, where the μ_A and μ_B are chosen so that

$$\overline{A(\mu)} = A(\mu_A), \quad \overline{B(\mu)} = B(\mu_B), \tag{7.6}$$

where the overbar indicates directional averaging.

$$\overline{f(\Theta)} = \int f(\Theta)\,S(\Theta)\,\mathrm{d}\Theta.$$

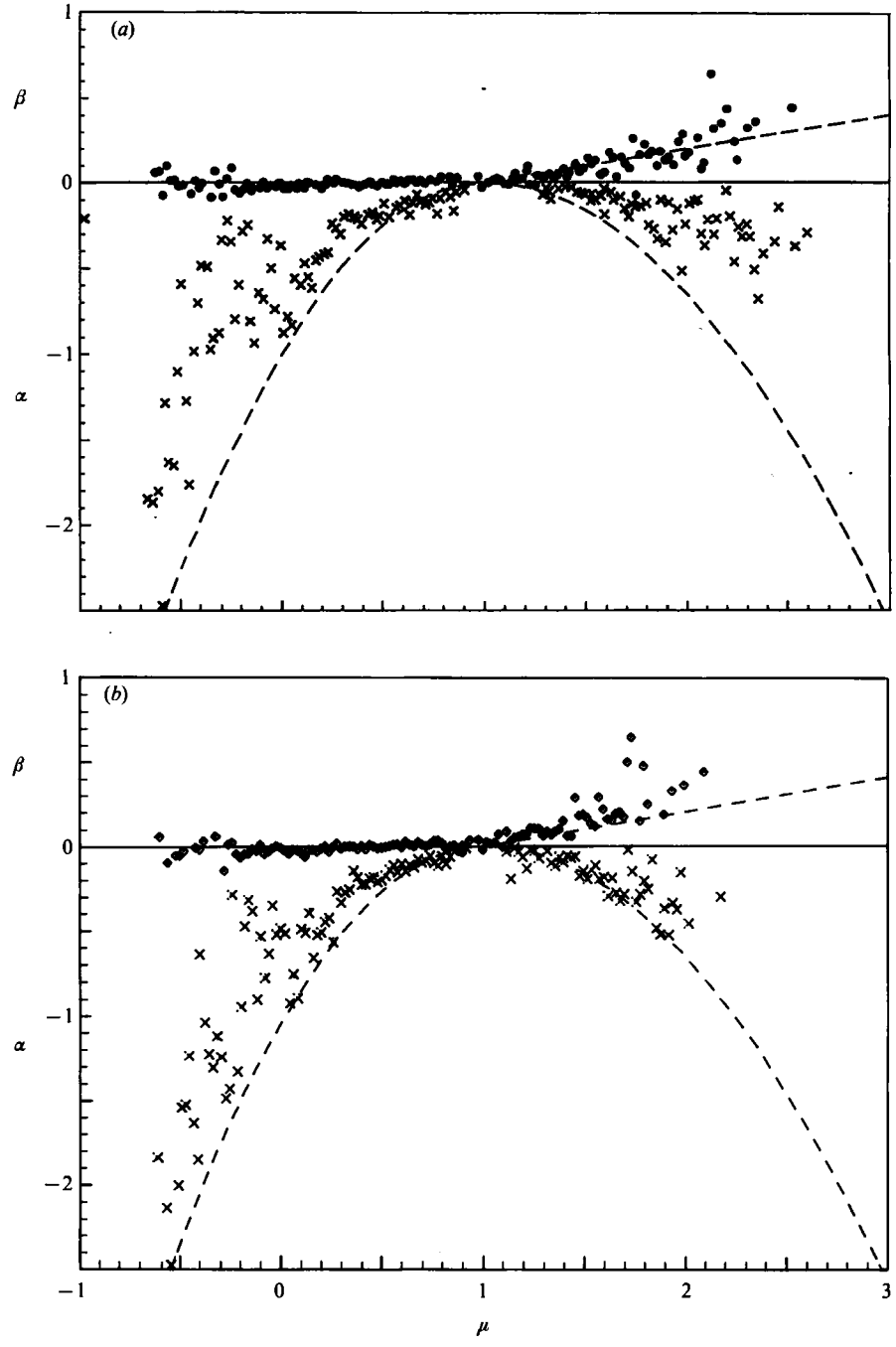

FIGURE 7. (*a*) Transfer function $\gamma(\mu, 0) = \alpha + \mathrm{i}\beta$ as function of μ for model 2 and all 77 and 81 data. ×, α; ●, β. Dotted lines are the relations (7.7), (7.8) found by Snyder *et al.* Points shown are interval averages. (*b*) As (*a*), except for model 4 and ◇, β.

Normally $\mu_A \neq \mu_B$; but we shall nevertheless omit the subscript unless confusion would otherwise arise. We also omit the hat in α and β.

The choice of μ_A and μ_B is not unambiguous, but is nevertheless rather straightforward if in addition to (7.4) the reasonable limit $\mu_A = \mu_B = \mu$ is demanded

for a unidirectional spectrum. Details are given in Appendix C, including a comparison of μ_B and the scale $\hat{\mu}$ employed by Snyder *et al.* (1981).

For further analysis of α *vs.* μ_A or β *vs.* μ_B the μ-axis for $-1 < \mu < 3$ was divided into 200 equal intervals and for each slot α and β were obtained as weighted means (with weights proportional to the inverse variance σ^{-2}). When the individual entries were consistent with a common mean we calculated the variances σ_α^2 and σ_β^2 in analogy with (6.16*a*), and otherwise with (6.16*b*). These variances were then used for weighting the data in (7.3).

We show the results for model 2 and model 4 in figure 7, where the dashed lines are

$$\beta = 0.2(\mu - 1) \quad \text{for } \mu > 0, \tag{7.7}$$

and

$$\alpha = -(\mu-1)^2 \qquad \text{for } \mu \leqslant 1$$

$$= -0.65(\mu-1)^2 \quad \text{for } \mu \geqslant 1, \tag{7.8}$$

which for model 1 corresponds to the results of Snyder *et al.* (1981).

The results for the other models look similar. The standard deviations of α and β are not included to avoid crowding. These deviations are of limited value in any case since for many points the individual entries contributing to the plotted mean values are not consistent with a common mean, as discussed above. Nevertheless the standard deviations are roughly what one would estimate from the scatter of the plots, namely $\sigma_\beta \approx 0.1$ for $\mu < 0$, $\sigma_\beta \approx 0.05$ for $0 \leqslant \mu \leqslant 1$ and $\sigma_\beta \approx 0.2$ for $\mu > 1$, whereas $\sigma_\alpha \approx 0.2$ for all μ.

The number of entries $n_\alpha(\mu)$ and $n_\beta(\mu)$ per μ-slot is typically 10–20 for $-0.1 < \mu < 1.3$ and decreases to $n \approx 3$ outside of this range. A characteristic feature of the $\mu_{A,B}$-algorithms (Appendix C) results in the crowding of entries $n_\beta \approx 50$, for $1 < \mu_B < 1.1$ and in the same range a thinning out of n_α, even to $n_\alpha = 0$ for $0.9 < \mu < 1.1$.

7.4. *Corrections for currents*

Since currents were not measured a true correction for these is impossible. To check the importance of such corrections we used tidal currents which are in the order of $|v| \approx 0.35$ m/s. We find that in our frequency range $f \leqslant 0.5$ Hz current corrections hardly influence our results, mainly because wind direction and current direction are not correlated. We have nevertheless included this correction in all of our final calculations. Details are given in Appendix A.

Corrections for wind drift are in the order of $v/c \approx 0.02U/c$ (Essen, Gurgel & Schirmer 1989) and from figure 7 we see $v/c < 0.05$. This will amount to a 10% reduction in the worst case for the wavenumber and leads to a sizeable correction in the vertical extrapolation. Again in the worst case (for $\mu \approx 2$ and $\lambda \approx 2$) this results in a 20% reduction of $|\gamma|$. On the other hand the correction for μ (Appendix A, A 4) is negligible.

7.5. *Directional distribution for swell and influence of the directional distribution*

We have discussed the case that both swell directions as determined by the array are admissible in §5, after (5.6). In this situation, which did not often occur, we chose that mean direction Θ_m as correct which yielded the better agreement between the measured real part α and the value $A(\mu_A)$ for model 1. Comparisons of consecutive directional distributions showed that our choice Θ_m did not result in an arbitrary switching of directions from run to run.

The results shown in figures 7 and 8 scatter considerably, especially in α. This

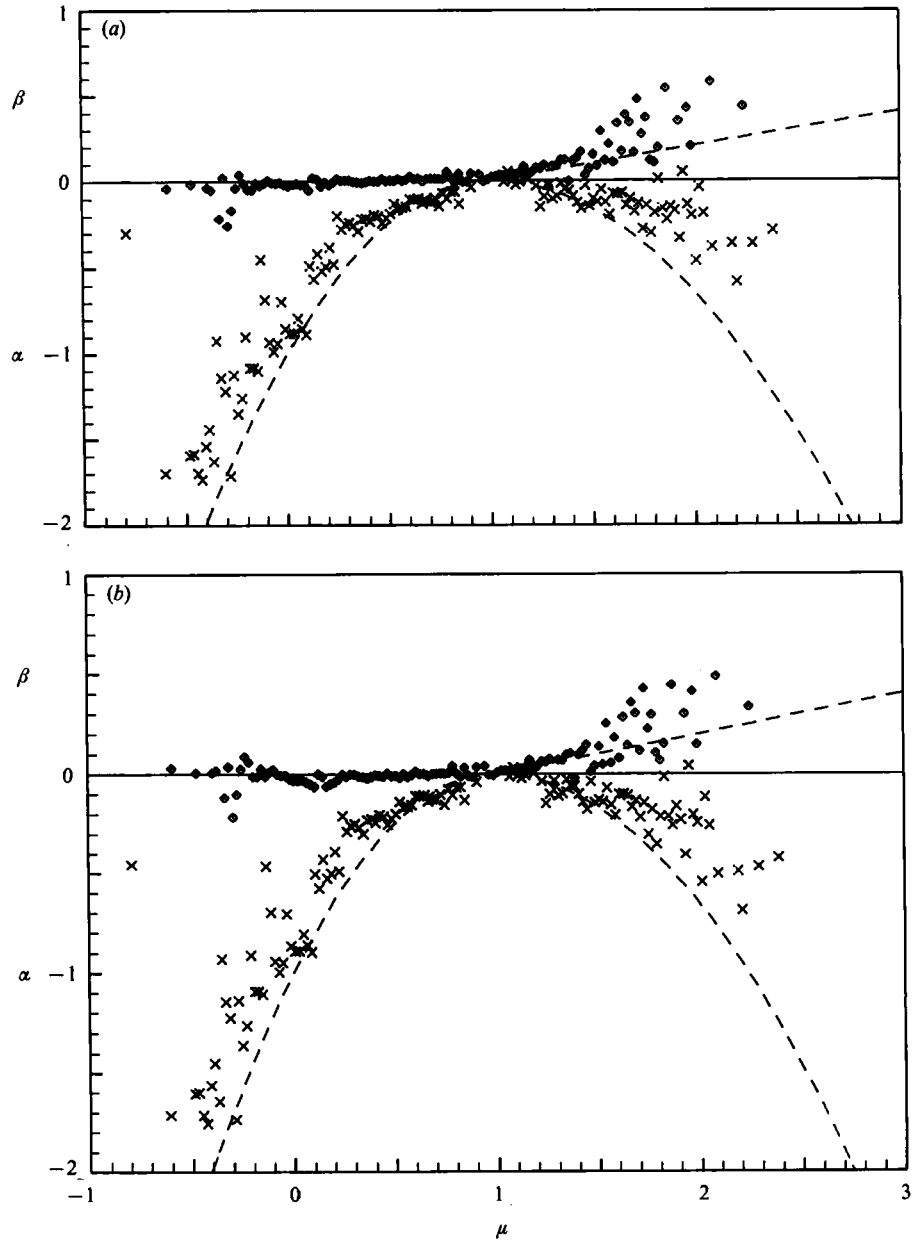

FIGURE 8. (*a*) As figure (*b*), but now for model 1 and 1977 data only. The reduced scatter in α is due to the better directional quality of the 1977-data. (*b*) As (*a*) model 1, 1977-data. We have now assumed a wind drift displacement of the resistance wire by $\hat{\Delta} = 0.30$ m into the wind direction.

scatter, particularly for negative μ associated with swell running against the wind, is mainly due to inadequate directional modelling in the 1981-experiment. From figure 7 (*a*), which shows more α-scatter than figure 7 (*b*) not all phase locked solutions were eliminated. With all 1981 data removed, as in figure 8 (*a*) the scatter in α is drastically reduced, and this is due to improved directional data rather than to differences in the models. We further tested whether the scatter of the α values was reduced, when we replaced the array information by pitch and roll information. In

a comparison using only those cases in which both sources of information were available, we could not detect any systematic differences between the two plots (not shown), and thus we conclude that the array information and the pitch and roll information are of roughly equal quality.

7.6. *Correction for displacements*

In §2.2.3 we have mentioned that on one occasion the resistance wire for the wave height ζ_1 was observed to slant leading to a 0.30 cm displacement between wave height and pressure measurements. We have used this rather extreme displacement in two tests. In the first we assume the wire to be displaced by $\hat{\Delta}$ in the downwind direction, calling this the wind drift displacement, in the second we assume it is displaced by $\hat{\Delta}$ in the direction of the tidal current. The corrections are negligible for the real part α of the transfer functions, and for β the effects are not as large as might be expected. Since tidal current and wave direction are nearly uncorrelated the effects should and do cancel for the current displacement (not shown).

The correction for wind drift displacement reduces the growth rate for waves running with the wind while for waves running against the wind the correction produces a small shift towards growth. The correction involves a factor corresponding to (7.1), but in view of the crudeness of the test we replace $S(\Theta)$ by the Dirac distribution $\delta(\Theta-\Theta_{\mathrm{m}})$ with the mean wave direction Θ_{m}, so that the change $\delta\beta$ of β is

$$\delta\beta = (k\hat{\Delta})\,\alpha\cos(\Theta_{\mathrm{m}}-\Theta_{\mathrm{U}})(1+O(k^2\hat{\Delta}^2)). \tag{7.9}$$

The approximation $S(\Theta)=\delta(\Theta-\Theta_{\mathrm{m}})$ should in most cases yield overestimates of $|\delta\beta|$. Only for some particular swell cases does (7.9) lead to an underestimate, in which case, however, $\delta\beta$ is small in any case (e.g. $\Theta_{\mathrm{m}}-\Theta_{\mathrm{U}}=\pm\frac{1}{2}\pi$). In figure 8 we show the results for model 1 and for 1977 data only, because there we have the more reliable directional information. We observe the predicted decrease in β for $\mu>0$ and the increase for $\mu<0$. The corrections are noticeable only for the highest few frequencies, are slightly smaller than $(k\hat{\Delta})\alpha$, owing to the directional factor, and as evident from figure 8 cause no grave problem regarding the measurement of γ.

The assumed displacement in the direction of the wind is an artificial worst-case model, used to test the sensitivity of our analysis. If anything, a displacement caused by the tidal current should be more realistic. The dip in β and $\mu\approx 0.2$ which is conspicuous in figure 8(*b*) can be traced to some persistent mean swell directions in light winds and is an artifact of our displacement assumption.

7.7. *Bias due to directional scatter*

Sampling and measurement error combine to produce a scatter of the directional parameters Θ_{m} and s around their true values. Concerning α, large errors in Θ_{m} will on average tend to increase small (true) values of $|\mu_A-1|$, and this should explain many of the differences between figures 7 and 8(*a*). On the other hand, for the smaller directional errors typical for the 1977 data, we were unable to identify a bias in $|\mu_A-1|$ (not shown). In Appendix C, we explain why we expect our μ_B values to be biased low.

In a crude approximation we obtain the bias as

$$\Delta\mu_B = \langle\mu_B\rangle-\mu_{\mathrm{Bt}} \approx -(\mu_{\mathrm{Bt}}-1)\langle\delta\Theta_{\mathrm{m}}^2\rangle^{\frac{1}{2}}, \tag{7.10}$$

where μ_{Bt} is the unbiased true value. Here $\langle\cdot\rangle$ denotes an ensemble average over an ensemble of realizations with the statistical properties of our measurements. In particular $\langle\delta\Theta_{\mathrm{m}}^2\rangle$ is the variance of the mean direction around the true value.

From our comparison of pitch and roll directional data with array data (not shown) we estimate

$$\langle \delta\Theta_m^2 \rangle \approx (\tfrac{1}{6}\pi)^2,$$

for all frequencies. If, in (7.3), b_1 is determined from a fit to the data, the fit to the bias corrected data would yield

$$b_{1c} = (1-\tfrac{1}{2}(\tfrac{1}{6}\pi)^2)\, b_1 \approx 0.85 b_1. \tag{7.11}$$

8. Discussion

8.1. *Regression analysis*

A regression analysis of the four models according to §7.2

$$\left.\begin{aligned} \alpha_i &= a_0 + a_1 A(\mu_{A,i}) + \epsilon_i, \\ \beta_i &= b_0 + b_1 B(\mu_{B,i}) + \epsilon_i, \end{aligned}\right\} \tag{8.1}$$

with A and B given in the Appendix yields the results shown in table 2. Since in all cases $a_0 = 0$ was consistent with the data we have omitted this entry. We have included standard errors in table 2, but these could be misleading. None of the regression fits is consistent in any strict sense and so assignment of standard errors is arbitrary.

The errors in table 2 have already been formally enlarged by increasing the errors of the bin averaged data to enforce consistency of the fits, but on the evidence presented in §7, we still believe some are too small. We suggest replacing the smaller error bounds by the informed guesses

$$\left.\begin{aligned} \Delta a_0 = 0.01 \quad \Delta a_1 = 0.1, \\ \Delta b_0 = 0.03, \quad \Delta b_1 = 0.05, \end{aligned}\right\} \tag{8.2}$$

and the slope b_1 should be corrected by multiplying by the bias factor 0.85, see (7.11). The effect of a wind drift displacement $\hat{\Delta} = 0.30$ m for model 4 yields negligible changes a_0, a_1, but for b_0 and b_1 we obtain

$$\left.\begin{aligned} b_0 &= 0.003, \\ b_1 &= 0.28, \end{aligned}\right\} \tag{8.3}$$

compared to $b_0 = -0.004$ and $b_1 = 0.37$ for $\hat{\Delta} = 0$. Results for the other models are similar. Since the assumed wind-drift displacement $\hat{\Delta} = 0.30$ m is rather extreme we consider the displacement errors to be contained in (8.2), but this is arbitrary.

We were unable to detect any dependence on parameters, such as significant wave height, $H_s = 4\langle\zeta^2\rangle^{\frac{1}{2}}$, gH_s/U^2, or mean square wave slope. However, not much effort was spent on these attempts, because in all circumstances the major effect of any data stratification was the increased scatter associated with smaller samples, so that no meaningful conclusions were possible.

The scatter of the α and β values is larger than the sampling error of a Gaussian process; it is also larger than expected from assignment of incorrect μ-values. While we have neglected some additional parameters, perhaps most notably (kz_0) and atmospheric stability (Janssen & Komen 1985), we cannot imagine such a dependence to be strong enough to explain the scatter. We estimate the roughly 5% scatter in the wave height measurements mentioned in §2.2.3 to lead to a scatter of about 1% in γ. In order to check this estimate we have for one test calculation made plausible corrections for the errors in ζ_1 and ζ_2. The largest changes $\delta\alpha$ in α are $|\delta\alpha|_{\max} = 0.06$

Model	Scaling velocity	a_1	b_0	b_1	Comparison model
1	U_5	0.70 ± 0.03	-0.01 ± 0.006	0.28 ± 0.08	SDEL, YS
2	u^*	0.70 ± 0.04	-0.05 ± 0.01	0.27 ± 0.1	—
3	$U(k^{-1})$	0.70 ± 0.02	-0.01 ± 0.003	0.30 ± 0.03	—
4	$U(k^{-1})$, u^*	0.71 ± 0.02	-0.004 ± 0.003	0.37 ± 0.02	P, MH
SDEL[a]	U_5	1.0 ± 0.1	0	0.2–0.3	1
P[b]	u^*	0	0	0.2	1
MH[c]	u^*	—	0	0.27	4
YS[d]	U_5	0.8 ± 0.2	—	—	1

Note: To correct for bias the regression values b_1 for Model 1–4 should be multiplied by 0.85.
[a] Snyder *et al.* (1981).
[b] Plant (1982).
[c] Mitsuyasu & Honda (1982).
[d] Young & Sobey (1985).

TABLE 2. Result of the regression analysis

(corresponding to a 5% error) and the changes in β are $|\delta\beta|_{\max} = 0.03$. The average effect is of the order of 1%, and negligible compared to other sources of scatter.

In retrospect, we would recommend the use of more robust statistical techniques, which are less sensitive to the assumption of a normal distribution.

8.2. *Discussion of results for* $\mu > 1$

In the wind-sea range some results stand out clearly, independent of the chosen model. For the imaginary part there is always a breakpoint near $\mu = 1$ but its position is not well enough defined to select a superior model. The growth rate obviously increases for $\mu > 1$, but we cannot decide whether this increase contains a quadratic term proportional to $\mu(\mu-1)$ as in model 4 or whether it is simply proportional to $(\mu-1)$. However, near $\mu = 1$ the increase does seem to be linear and not proportional to $(\mu-1)^2$ as has been suggested by Hsiao & Shemdin (1983) and Al-Zanaidi & Hui (1984).

The measured growth rates are in agreement with those reported by Snyder *et al.* (1981), which in turn also roughly agree with the most recent laboratory measurements by Papadimitrakis *et al.* (1986). Snyder *et al.* find

$$\beta = b(\mu-1),$$
$$b = 0.2-0.3, \tag{8.4}$$

as compared to our bias corrected value

$$b_1 = 0.25\pm0.07. \tag{8.5}$$

The bias corrected value for model 4, $b_1 = 0.31$ is higher than the values reported by Plant (1982) and Mitsuyasu & Honda (1982), but the comparison really only tests the low end of the interpolation function ψ_4, see Appendix B, connecting high values of $\mu \approx 25$ and our small values $\mu < 2$.

The results (8.4) and (8.5) yield growth rates about twice as high as predicted by Makin (1979, 1980, 1981, 1982, 1983*a*, *b*), Makin & Chalikov (1980) and parameterized by Chalikov as

$$\beta_C = 0.12\left(25\frac{u_*}{c}-1\right), \tag{8.6}$$

which is roughly of the same size as the result of Miles, depending somewhat on $\Omega_0 = gz_0/u_1^2$ (where $u_1 = u^*/\kappa$), as may be seen from the plots of Snyder *et al.* (1981) (their figure 9) and the parameterization of Miles' results given by Janssen & Komen (1985). Finally Jacobs (1987) predicts (for $|\cos\Theta| = 1$)

$$\beta_J = 2\kappa\frac{u_*}{c}\left(\frac{U}{c}-1\right) \approx 0.03\frac{U}{c}\left(\frac{U}{c}-1\right). \tag{8.7}$$

For the real part α our value $a_1 = 0.7 \pm 0.1$ is smaller than the $a_1 \simeq 1$ found by Snyder *et al.* There may be some bias due to directional errors but we were unable to demonstrate its presence for $\mu > 1$. We note that our values for α agree better with the results of the simplified analysis of Snyder *et al.* than with those of their general model, see their figure 22. Their figure 9 shows to what extent Miles' predictions for α depend on $\Omega_0 = gz_0/u_1^2$ and the fairly good agreement with Townsend's (1972) calculations (his table 2) indicates that α is not very sensitive to details of turbulence closure. While the visual impression of the α, β plots may favour one particular model there is really no objective basis for such a selection. Perhaps model 1 should be discounted on theoretical grounds.

Thus, concerning the more or less linear increase of the growth rate β the measurements do not contradict the theories mentioned after (8.6), nor those of Townsend (1972) or Gent & Taylor (1976), but all the theories yield β about half as large as measured; all theories are adjustable to some extent and given the error margin the gap between theory and experiment seems to be bridgeable. The exception is β_J (8.7), being too small by a factor of 5–10. Townsend (1980) has also suggested an alternative theory in which β is too large by a factor of about 2 (his figure 6*a*). This is not obviously in disagreement with our measurements, but the disparity is heightened to a factor of about 3 if the theoretically predicted dependence on λ instead of the exponential decay is used in the extrapolation to the surface; we refer to the discussion after (6.9). Thus Townsend's (1980) theory is in disagreement with the measurements, provided the predicted vertical decay at $\mu = 2$ (his figure 7*a*) is representative for other values of μ.

If we accept the μ-dependent vertical extrapolation (6.12), we estimate an average correction factor $\delta r \simeq 0.6$, with $\delta r = 1$ at $\mu = 1$ and $\delta r \approx \exp(-0.3 \times 2.3) = 0.53$ at $\mu = 2$, $\lambda_1 = 2.3$. The well-established linear growth near $\mu = 1$ would hardly be affected, while the values of α and β near $\mu = 2$ would be roughly halved. Qualitatively agreement with (8.6) would be improved, at the expense of an inexplicable vertical behaviour. The disagreement with Hsiao & Shemdin (1983) would remain, and we would have smaller α and β values than Snyder *et al.* (1981).

If we take into account the current correction for wind drift as discussed in §7.4 we come into closer agreement with theory, since the β values at $\mu \approx 2$ are then reduced by about 20%, and figure 9 of Snyder *et al.* (1981) shows that the α-values would then also agree better with Miles' theory. However, α would also depart more strongly from the experimental values of Snyder *et al.* (1981), as can be seen from figures 7 and 8.

8.3. *Discussion of the results for $\mu < 1$*

In the range $\mu < 1$ our data show neither significant decay or growth. Our best guess is $b_0 = -0.01 \pm 0.03$ but it would be hazardous to speculate on the sign of b_0; $|\beta| \leqslant 0.03$ is all we can really say. Snyder *et al.* (1981) find a phaseshift ϕ of essentially 180°, while Young & Sobey (1985) report $\phi = 177° \pm 6°$ from laboratory measurements. (Young & Sobey report $\phi_{YS} = 183°$, but their phase convention is $\tan\phi_{YS} = -\beta/\alpha$,

ours is $\tan\phi = \beta/\alpha$. A further convention found in the literature is Gent's $\tan\phi_G = \beta^{-1}\alpha(\boldsymbol{U}\cdot\boldsymbol{k})/Uk$.) The mean value of 177° would actually, if it differed significantly from 180° indicate a weak growth, whereas we would intuitively, and in agreement with all theories except for Miles (1957) and Benjamin (1959), expect weak decay. Dobson (1971*b*) reported much higher damping rates $\beta \approx -0.3$, but these were obtained from very few data. Snyder (1974) finds large phaseshifts $\phi_s \approx 200°$ near $\mu = 1$, from which the decay is difficult to infer, because $|\gamma|$ is very small near $\mu = 1$. He also finds $\phi_s \approx 200°$ near $\mu = -1$ which would correspond to very large damping rates $\beta \approx -2.0$. As stated in Snyder *et al.* (1981) these earlier results are not supported by later measurements in the Bight of Abaco. (Incidentlly we mention that the damping mechanism invoked by Young & Sobey (1985) due to turbulent stress $\tau_1 = \langle \tilde{u}_1 \tilde{u}_1 \rangle$, where $\tilde{u}_1$ is the wave induced horizontal velocity fluctuation cannot contribute, since $\langle \zeta \tau_1 \rangle = 0$, owing to $\langle \exp(\mathrm{i}(kx - \sigma t)) \rangle = 0$.)

For the real part α we find $a_1 = 0.7 \pm 0.1$, while Young & Sobey (1985) find $a_1 = 0.8 \pm 0.2$. We had chosen (7.4) with the intention that $a_1 = 1.0$ should describe the results of Snyder *et al.* (1981), but our choice is somewhat unfortunate, since the fit α_s shown in their figure 22 has $\alpha_s \approx a_s(\mu)A(\mu)$ with $a_s(-1) \approx 0.8$, $a_s(-0.5) \approx 0.9$ and $a_s(\mu) \approx 1$ for $\mu > 0$. Thus our value $a_1 = 0.7$ is considerably lower than a_s for $-0.5 < \mu$, but deviates only slightly for $\mu < -0.5$. We thus have fairly good agreement with Young & Sobey (1985), but some conflict with the Bight of Abaco results. Differences could be attributed to a bias due to directional errors, but the evidence is inconclusive; see §7.5.

For comparison with theory, we note that both for $(kz_0) \to 0$ and for $u_*/c \to 0$ we should expect the theoretical results to approach those for potential theory, thus we expect $\beta \to 0$ and $a_1 \to 1$. Calculations summarized in Chalikov (1986) agree with the expectation for β

$$\left.\begin{aligned} \beta &= 32\frac{u_*}{c}\left(\frac{u_*}{c} - 0.04\right) \quad \text{for } 0 < \frac{u_*}{c} < 0.04, \\ \beta &= 13\frac{u_*}{c}\left(\frac{u_*}{c} + 0.08\right) \quad \text{for } -0.04 < \frac{u_*}{c} < 0, \\ \beta &= -0.02 \qquad\qquad\qquad \text{for } \frac{u_*}{c} < -0.04. \end{aligned}\right\} \tag{8.8}$$

While our data do not support this prediction they do not conflict with it either. For $\mu < 0$, Al-Zanaidi & Hui (1985) made the prediction

$$\beta_{AH} = -0.04\left(\frac{U(k^{-1})}{c} - 1\right)^2. \tag{8.9}$$

Although we have not properly tested this model it does not seem to fit our data, although the scatter at $\mu = -0.8$ might make it acceptable. We note that (8.9) does not conform with our expectations for $u^*/c \to 0$. We point out, that Al-Zanaidi & Hui (1985) do not show any calculations for $-0.8 < U(k^{-1})/c < 0.5$, limitations which also apply for Gent (1977). For the range of parameter values covered the two calculations do not differ strongly, and in fact do not contradict our measurements. No matter how we extend (8.7) to $\mu < 0$ (Jacobs (1987) suggests damping), the data provide little support in either case. As with (8.9) the scatter of the data might save β_J for $\mu < 1$.

In contrast to (8.9) Gent (1977) expects his calculations to yield $\beta \to 0$ for $u_*/c \to 0$, which agrees with (8.8). At $u_*/c = 0.01$ Chalikov (1986) finds $\beta = -0.01$. This damping is still stronger than the rates deduced by Snodgrass *et al.* (1966, their table 5), who find $-3 \times 10^{-3} < \beta < 0$ at $f = 0.06$ Hz, corresponding to $E^{-1}\,\mathrm{d}E/\mathrm{d}x < 0.05$ dB/deg. One may ask whether the limit $u_*/c \to 0$ depends strongly on kz_0 and whether our data, taken at $f > 0.11$ Hz really compare with data measured at $f \approx 0.06$ Hz.

For the real part α the theoretical situation should be simpler and we should expect $u^*/c \to 0$ to be an uncomplicated limit. It is presumably for this reason that Chalikov shows no results for small values of u_*/c. However, within the range of values covered by their calculations, Al-Zanaidi & Hui (1985) typically find $a_1 = 0.75$ (their $\delta_r = -\delta_i/\sin\Phi \approx 0.75$ for $\delta_i = -0.04$ and $\Phi = 183°$) and from Gent (1977, his table 5) we find $a_{1g} = 0.80$ for $c/u_* = -22$, $R = 10$, and $a_{1g} = 0.91$ for $c/u_* = -36$, $R = 11$; ($|\gamma| = 3.95$ and $|\gamma| = 2.80 = 7250/(2 \times 36^2)$); the last equation indicating how to convert the tabulated values to our normalization.

Thus the results of calculations for $|U/c| > 0.5$ are in fair agreement with the data of Young & Sobey (1985), Snyder *et al.* (1981) and this experiment. But in contrast to our data and those of Young & Sobey (1985), those of Snyder *et al.* (1981) do indicate $a_1 \to 1$ for $u_*/c \to 0$.

At present we cannot be sure at which values of u_*/c theory begins to show the expected approach $a_1 \to 1$, but Gent's (1977) value of $a_1 = 0.91$ gives an indication that it should occur near $|U/c| = 0.8$.

9. Summary and conclusions

Two experiments in 1977 and 1981 yielded about 90 h of data of simultaneous air pressure and wave height measurements. The pressure measurements were made at two heights on a thin needle-structure at fixed heights over mean water level ranging from 0.70–6.50 m. Waves were measured with two resistance wires, an underwater pressure sensor and pitch and roll buoys. Wind velocity was measured with a cup and vane anemometer with speeds U between 2 and 12 m/s.

We estimate errors caused by reflected waves and flow disturbance by the structure to be negligible. The purpose of the experiment was to determine the dependence of the spectral pressure transfer coefficient

$$\gamma = \alpha + \mathrm{i}\beta = \frac{1}{\rho_a}\frac{1}{kc^2}\langle p_a \zeta^* \rangle / \langle \zeta \zeta^* \rangle$$

on the variables $\mu = U\cos\Theta/c$ and $\lambda = kz$.

Owing to limitations arising from fixed pressure sensor heights and relatively small horizontal distances between the wave sensors we have restricted our spectral analysis to frequencies $\frac{14}{128} < f < 0.5$ Hz, to $-1 < \mu < 2.5$ and to $\lambda < 2.3$.

We limited the directional description of the wave field to a $\cos^{2s}(\frac{1}{2}(\Theta - \Theta_m))$ model and in general the agreement between array results and pitch and roll results was satisfactory.

The vertical dependence of $\gamma(\mu, \lambda)$ was essentially exponential, $\gamma(\mu, \lambda) = \gamma(\mu, 0)\,\mathrm{e}^{-\lambda}$. Deviations from an exponential decay are to be expected and were observed. In our opinion, the observed deviations are due to some unidentified bias of the analysis procedure and have no physical significance. For this reason we have used $\exp(-\lambda)$ in the extrapolation to the surface. If instead we assume the exponential decay constant to depend on μ as given by (6.12) the values for $\gamma(\mu, 0) = \alpha + \mathrm{i}\beta$ will be

reduced by a factor $\delta r \approx 0.6$ if $\mu > 1$. The consequences of such an assumption are discussed in §8.2.

For exponential decay according to $\exp(-\lambda)$ our results are consistent with those reported by Snyder *et al.* (1981); for the imaginary part β we obtain

$$\beta = (0.25 \pm 0.07)(\mu - 1) \quad \text{for } 1 \leqslant \mu \leqslant 2.5,$$
$$\beta = 0 \quad \text{otherwise.}$$

Other parameterizations for β are also consistent with the data but especially for values $\mu \approx 1$ a linear increase of β seems to be well established, and accordingly for $1 < \mu < 1.5$ our growth rates are larger than those observed by Hsiao & Shemdin (1983, 1985). In the swell range $\mu < 1$ the data are consistent with $\beta = 0$, in agreement with Snyder *et al.* (1981) and Young & Sobey (1985).

For the real part of α we obtain $\alpha = (0.7 \pm 0.1) A$ where A is given by (7.4) and models the result of Snyder *et al.* (1981) for $\mu > -0.5$. We believe the factor (0.7 ± 0.1) to be biased low, but the data are ambiguous. In the swell range, particularly for $-1 < \mu < 0$, our possibly biased results are consistent with the laboratory data of Young & Sobey (1985). For $\mu < -0.5$ our results are roughly in agreement with the results of Snyder *et al.* (1981).

The assignment of μ-values to the spectra hinges on the directional resolution and it is difficult to estimate how much uncertainty is introduced by inadequately resolved directional spectra. Compared to these, other sources of error, such as displacement errors, errors due to currents or effects due to flow interference should be minor.

We express our thanks to R. Snyder for generously providing us with his pressure probes and to F. Dobson for useful advice in many discussions. Special thanks are due to M. Dunckel (Max-Planck-Institut für Meteorologie) who was responsible for the experimental and electronic side of the programme, to K. Richter and H. Carlson (Deutsches Hydrographisches Institut) for the wave measurements and to M. Grünewald (Meteorologisches Institut) for data handling. This work was supported by Deutsche Forschungsgemeinschaft through a grant to SFB 94.

Appendix A. Correction for tidal currents

A correct calculation would require retaining the angular dependence of the length of the wavenumber $k(\omega, \Theta)$ in modelling the directional data D_α (5.4),

$$D_\alpha(\omega) = \int \exp(\mathrm{i}k(\omega, \Theta) L_a \cos\Theta) S(\omega, \Theta)\, \mathrm{d}\Theta. \tag{A 1}$$

The array is assumed oriented with $\Theta = 0$. For a current $\boldsymbol{v} = v(\cos\phi, \sin\phi)$, $v(z) = v = \text{const}$ and lowest-order estimates $k_0 = \omega^2/g$, $c_0 = g/\omega = \omega/k_0$ we have to first order in $\epsilon = v\cos(\Theta - \phi)/c$

$$k(\omega, \Theta) = k_0(1 - 2\epsilon). \tag{A 2}$$

In our estimates of $S(\omega, \Theta)$ we have set $k(\omega, \Theta) = k_0(\omega)$, which for frequencies at $f \approx 0.5$ Hz is fairly crude since here typically $\epsilon \approx 0.1$. Nevertheless, in view of our insecure knowledge of $\boldsymbol{v}$ and the limitation to a two-parameter fit of $S(\omega, \Theta)$ in any case, we felt it was not worthwhile to recalculate $S(\omega, \Theta)$. Thus we retain $S(\omega, \Theta)$ as an approximation to the true normalized directional distribution as observed in our observational frame for which $v \neq 0$.

To model the measured estimates of the transfer function $\gamma(\mu)$, which are directionally integrated values, we must evaluate integrals such as

$$\bar{f} = \int f(\mu(\omega, \Theta))\, S(\omega, \Theta)\, \mathrm{d}\Theta, \tag{A 3}$$

where

$$\mu(\omega, \Theta) = \frac{\boldsymbol{k}(\hat{\boldsymbol{U}} - \boldsymbol{v})}{\sigma}, \tag{A 4}$$

and $\sigma = (kg)^{\frac{1}{2}}$. To first order in ϵ we have from (A 2)

$$\mu = (1-\epsilon)\frac{U}{c_0}\cos(\Theta - \Theta_{\mathrm{u}}), \tag{A 5}$$

where

$$\boldsymbol{U} = (\hat{\boldsymbol{U}} - \boldsymbol{v}) = U(\cos\Theta_{\mathrm{U}}, \sin\Theta_{\mathrm{U}}).$$

As mentioned in §4, throughout the paper the frame of reference in which the current vanishes is used, thus $\hat{\boldsymbol{U}}$ is the measured velocity and correspondingly, for instance in (B 5) U/c is to be read as $(1-\epsilon)\,U/c_0$ and u_1/c as $(1-\epsilon)\,u_1/c_0$. For tidal, but not for wave-induced currents the effect of (A 2) was taken into account in the extrapolation of γ values to the surface.

Appendix B. Description of the models

Models 2 and 3 use $A(\mu)$ and $B(\mu)$ as given in (7.4) and (7.5), but differ in the velocity scale.

Model 2

$$\mu_2 = \frac{1}{C_{\mathrm{D,M}}^{\frac{1}{2}}}\frac{u_*}{c}\cos\Theta \tag{B 1}$$

$$u_* = C_{\mathrm{D}}^{\frac{1}{2}}\, U_5 \tag{B 2}$$

$$C_{\mathrm{D}} = (0.91 + 0.078U_5)\,10^{-3} \quad \text{(Wu 1982)} \tag{B 3}$$

where U_5 is given in [m/s] and $C_{\mathrm{D,M}} = C_{\mathrm{D}}(U_5 = 5\ \mathrm{m/s})$.

This model was tested, because it has been used in recent wave prediction models, see Komen, Hasselmann & Hasselmann (1984) and Janssen, Komen & Voogt (1987).

Model 3

$$\mu_3 = \frac{U(k^{-1})}{c}\cos\Theta$$

and $U(k^{-1})$ is obtained from U_5 by (B 2) and a logarithmic wind profile.

Model 4

$$A_4(\mu) = A(\mu_3), \tag{B 4}$$

$$B_4(\mu) = w_1\frac{u_1}{c}\cos\Theta\left\{\frac{U(k^{-1})}{c}\cos\Theta - 1\right\} = w_1\psi_4(\mu) \quad \text{for } \mu_3 > 1, \tag{B 5}$$

$$B_4(\mu) = 0 \quad \text{for } \mu_3 < 1,$$

$$u_1 = 2.5u_*.$$

This model is similar to the first three for $U/c < 2$ and joins smoothly with models proposed for high values of U/c as for instance,

$$\beta_{\mathrm{PM}} = w_0\left(\frac{u_*}{c}\right)^2 \tag{B 6}$$

Plant (1982) finds $w_0 = 33$, Mitsuyasu & Honda find $w_0 = 45$. Hsiao & Shemdin (1983) have proposed

$$\beta_{\mathrm{HS}} = 0.12\left(\frac{U_{10}}{c}\cos\Theta - 1\right)^2$$

which is similar to (B 6) for large U/c.

For $\cos\Theta = 1$, $w_0/w_1 = 33$ and $\Omega_0 = gz_0/u_1^2 = 3\times10^{-3}$ (B 5) and (B 6) join with continuous slope at

$$\frac{u_1}{c} = 0.5, \quad \text{i.e.} \quad \frac{U(k^{-1})}{c} = 3.6.$$

The value for Ω_0 is consistent with (B 3).

To maintain a formal similarity in the plots we use

$$\left.\begin{aligned} &\mu_{4B} = \mu_{3B} \quad \text{for } B_4 \leqslant 0, \\ &\mu_{4B} - 1 = 5\psi_4 \quad \text{for } B_4 \geqslant 0, \end{aligned}\right\} \tag{B 7}$$

with ψ_4 given by (B 5). With this choice

$$\beta = b_0 + b_1(\mu_{4B} - 1)$$

will join smoothly to Plant's formula (B 6) for $b_1 = 0.2$ and $b_0 = 0$, corresponding to $w_0/w_1 = 33$. This model we formulated as a rough description of Miles' (1957, 1959) results, also see Stewart (1974), Janssen & Komen (1985), whereas Jacobs (1987), (8.7), presents an independent theoretical derivation.

Appendix C. Calculation of equivalent μ-values

First the current corrections are applied as explained in Appendix A. For any given reference wind speed U_{r} we define for models 1–3

$$\mu_B - 1 = \int(\mu - 1)\,S(\Theta)\,\mathrm{d}\Theta \quad \text{if } (\mu - 1) \leqslant 0 \text{ for all } \Theta \tag{C 1}$$

and

$$\mu_B - 1 = \int_{\mu>1}(\mu - 1)\,S(\Theta)\,\mathrm{d}\Theta \quad \text{otherwise,} \tag{C 2}$$

while for model 4 according to (B 5), we use (C 1) if its side conditions are met, and otherwise (C 2) is replaced by

$$\mu_B - 1 = 5\int_{\psi_4>0}\psi_4(\mu)\,S(\Theta)\,\mathrm{d}\Theta. \tag{C 3}$$

For μ_A we have

$$(\mu_A - 1) = -(H_- + q^2H_+)^{\frac{1}{2}} \quad \text{for } H_- > H_+ \tag{C 4}$$

and

$$(\mu_A - 1) = \frac{1}{q}(H_- + q^2H_+)^{\frac{1}{2}} \quad \text{for } H_- < H_+ \tag{C 5}$$

with $q^2 = 0.65$ and

$$H_- = \int_{(\mu-1)<0} (\mu-1)^2 S(\Theta)\,\mathrm{d}\Theta, \tag{C 6}$$

while in H_+ the integral runs over the domain $(\mu-1) > 0$.

We now compare our approach (C 2) to the method applied by Snyder *et al.* (1981) in their simplified analysis.

For the same truncated $\cos^2\Theta$ distribution as used by Snyder *et al.* (1981) to obtain their $\hat{\mu} = 8/(3\pi)\,U/c = 8/(3\pi)\,\mu_0$ we obtain μ_B as

$$\mu_B = \frac{2}{\pi}\left\{\tfrac{4}{3}(\mu_0^2-1)^{\frac{1}{2}} - \frac{1}{3}\frac{(\mu_0^2-1)^{\frac{1}{2}}}{\mu_0^2} + \arcsin\left(\frac{1}{\mu_0}\right)\right\}, \tag{C 7}$$

which rapidly approaches $\hat{\mu}$ for $\mu_0 \gg 1$, such that $\mu_B = \hat{\mu}(1+\frac{1}{5}\mu_0^{-4},\ldots)$, while for $\mu_0 - 1 \ll 1$ we find

$$\mu_B - 1 = x(\hat{\mu}-y)^{\frac{3}{2}} = 1.25(\hat{\mu}-0.85)^{\frac{3}{2}}, \tag{C 8}$$

where $y = 8/(3\pi)$ and $x = y^{-\frac{3}{2}}13\sqrt{2}/(6\pi)$. Perhaps we can see just a trace of a linear relation $b(\mu_B-1)$ at $\mu \approx 1$ in figures 6 and 7 of Snyder *et al.* (1981).

To calculate the error in μ_B (C 2) arising from errors in the directional distribution we observe that for $\langle\Theta_\mathrm{m}-\Theta_U\rangle = 0$ the bias $\Delta\mu_B$ arising from errors $\delta\Theta_\mathrm{m}$ is much larger than the one caused by errors in the sharpness s and a Taylor expansion yields

$$\Delta\mu_B = \frac{1}{2}\frac{\partial^2\mu_B}{\partial\Theta_\mathrm{m}^2}\langle\delta\Theta_\mathrm{m}^2\rangle, \tag{C 9}$$

$$\frac{\partial^2\mu_B}{\partial\Theta_\mathrm{m}^2} = \frac{U}{c}\int_{-\Theta_1}^{\Theta_1} \sin\Theta\frac{\partial S(\Theta)}{\partial\Theta}\,\mathrm{d}\Theta = \mu_B'' \tag{C 10}$$

with $\cos\Theta_1 = c/U$. For $U/c \approx 1$ when $\Theta_1 \ll \Delta_2$, where Δ_2 is the angular spread of $S(\Theta)$ – for (5.2) $\Delta_2 = (2/(s+1))^{\frac{1}{2}}$, see Longuet-Higgins *et al.* (1963) – we have $\mu_B'' \sim \Theta_1^3$, whereas for $\Theta_1 \gg \Delta_2$, $\mu_B'' \to -\mu_B$. In a very crude approximation simulating the Θ_1 dependence by the factor $(1-c/U)$, we obtain

$$\mu_B'' \approx -\frac{U}{c}q_1\left(1-\frac{c}{U}\right) = -\left(\frac{U}{c}-1\right)q_1 \approx -(\mu_B-1), \tag{C 11}$$

with $q_1 = s/(s+1)$.

REFERENCES

Al-Zanaidi, M. A. & Hui, W. H. 1984 Turbulent airflow over water waves – a numerical study. *J. Fluid Mech.* **148**, 225–246.

Abramowitz, M. & Stegun, I. A. 1965 Handbook of Mathematical Functions. Dover.

Barber, N. F. & Ursell, F. 1948 The generation and propagation of ocean waves and swell. 1. *Phil. Trans. R. Soc. Lond.* A **240**, 527–560.

Benjamin, T. B. 1959 Shearing flow over a wavy boundary. *J. Fluid Mech.* **6**, 161–205.

Chalikov, D. V. 1986 Numerical simulation of the boundary layer above waves. *Boundary-Layer Met.* **34**, 63–98.

Dobson, F. W. 1971*a* Measurements of atmospheric pressure on wind-generated sea waves. *J. Fluid Mech.* **48**, 91–127.

Dobson, F. W. 1971*b* The damping of a group of sea waves. *Boundary-Layer Met.* **1**, 399–410.

Dobson, F. W. 1985 Comment on 'Measurements of wind velocity and pressure with a wave follower during MARSEN', by S. V. Hsiao and O. H. Shemdin. *J. Geophys. Res.* **90**, C5, 9206–9208.

DOBSON, F. W. & ELLIOTT, J. A. 1978 Wave-pressure correlation measurements over growing waves with a wave follower and fixed-height pressure sensors. In *Turbulent Fluxes through the Sea Surface, Wave Dynamics, and Prediction* (ed. A. Favre & K. Hasselmann), pp. 421–432. Plenum.

DONELAN, M. A., HAMILTON, J. & HUI, W. H. 1985 Directional spectra of wind-generated waves. *Phil. Trans. R. Soc. Lond.* A **315**, 509–562.

ELLIOTT, J. A. 1972 Microscale pressure fluctuations near waves being generated by the wind. *J. Fluid Mech.* **54**, 427–448.

ESSEN, H. H., GURGEL, K. W. & SCHIRMER, F. 1989 Surface currents in the Norwegian Channel. *Tellus* **41A**, 162–175.

GENT, P. R. 1977 A numerical model of the air flow above water waves. Part 2. *J. Fluid Mech.* **82**, 349–369.

GENT, P. R. & TAYLOR, P. A. 1976 A numerical model of air flow above water waves. *J. Fluid Mech.* **77**, 105–128.

GÜNTHER, H. W., ROSENTHAL, R. & RICHTER, K. 1979 Application of the parametrical wave prediction model to rapidly varying wind fields during JONSWAP 1973. *J. Geophys. Res.* **84**, 4855–4864.

HASSELMANN, D., BÖSENBERG, J., DUNCKEL, M., RICHTER, K., GRÜNEWALD, M. & CARLSON, H. 1986 Measurements of wave-induced pressure over surface gravity waves. In *Wave Dynamics and Radio Probing of the Ocean Surface* (ed. O. M. Phillips & K. Hasselmann), pp. 353–368. Plenum.

HASSELMANN, D. E., DUNCKEL, M. & EWING, J. A. 1980 Directional wave spectra observed during JONSWAP 1973. *J. Phys. Oceanogr.* **10**, 1264–1280.

HASSELMANN, K. *et al.* 1973 Measurements of wind wave growth and swell decay during the Joint North Sea Wave Project (JONSWAP). *Ergänzungsheft z. Deutsch. Hydrogr. Ztschr.* A, no. 12.

HSIAO, S. V. & SHEMDIN, O. H. 1983 Measurements of wind velocity and pressure with a wave follower during MARSEN. *J. Geophys. Res.* **88**, C14, 9841–9849.

HSIAO, S. V. & SHEMDIN, O. H. 1985 Reply (to F. W. Dobson). *J. Geophys. Res.* **90**, C5, 9209–9210.

HSU, C. T., WU, H. Y., HSU, E. Y. & STREET, R. L. 1982 Momentum and energy transfer in wind generation of waves. *J. Phys. Oceanogr.* **12**, 929–951.

JACOBS, S. J. 1987 An asymptotic theory for the turbulent flow over a progressive water wave. *J. Fluid Mech.* **174**, 69–80.

JANSSEN, P. A. E. M. & KOMEN, G. J. 1985 Effect of atmospheric stability on the growth of surface gravity waves. *Boundary-Layer Met.* **32**, 85–96.

JANSSEN, P. A. E. M., KOMEN, G. J. & VOOGT, W. J. P. DE 1987 Friction velocity scaling in wind wave generation. *Boundary-Layer Met.* **38**, 29–35.

JEFFREYS, H. 1924 On the formation of waves by wind. *Proc. R. Soc.* A **107**, 189–206.

KATO, H. & SANO, K. 1971 An experimental study of the turbulent structure of wind over water waves. *Rep. Port Harbour Res. Inst.* **10**, 3–42.

KAWAI, S. 1979 Generation of initial wavelets by instability of a coupled shear flow and their evolution to wind waves. *J. Fluid Mech.* **93**, 661–703.

KENDALL, J. M. 1970 The turbulent boundary layer over a wall with progressive surface waves. *J. Fluid Mech.* **41**, 259–281.

KOMEN, G. J., HASSELMANN, S. & HASSELMANN, K. 1984 On the existence of a fully developed wind-sea spectrum. *J. Phys. Oceanogr.* **14**, 1271–1287.

KONDO, J., FUJINAWA, Y. & NAITO, G. 1972 Wave-induced fluctuation over the sea. *J. Fluid Mech.* **51**, 751–771.

LAI, R. J. & SHEMDIN, O. H. 1971 Laboratory investigation of air turbulence above simple water waves. *J. Geophys. Res.* **76**, 7334–7350.

LONG, R. B. 1980*a* The statistical evaluation of directional spectrum estimates derived from pitch/roll buoy data. *J. Phys. Oceanogr.* **10**, 944–952.

LONG, R. B. 1980*b* A parametrical model for the vertical structure of the induced atmospheric pressure field above a spectrum of surface gravity waves. *J. Fluid Mech.* **99**, 163–183.

LONGUET-HIGGINS, M. S., CARTWRIGHT, D. E. & SMITH, N. D. 1963 Observations of the directional

spectrum of sea waves using the motions of a floating buoy. In *Ocean Wave Spectra*, pp. 111–136. Prentice Hall.

McLean, J. W. 1983 Computation of turbulent flow over a moving wavy boundary. *Phys. Fluids* **26**, 2065–2073.

Makin, V. K. 1979 The wind field over waves. *Okeonologia* **19**, 206–212 (Engl. transl. *Oceanology* **19**, 127–130).

Makin, V. K. 1980 Some results of numerical modelling of laboratory experiments to investigate the structure of air flow above waves. *Izv. Akad. Nauk. SSSR. Fiz. Atmos. Okeana* **16**, 989–991 (Engl. transl. *Izv. Atmos. Ocean. Phys.* **16**, 732–734).

Makin, V. K. 1981 Interaction of swell waves with head winds. *Meteorologia i Gidrologia* **11**, 95–97 (Engl. transl. *Sov. Met. Hydrol.* **11**, 79–81).

Makin, V. K. 1982 Numerical studies of wind–wave interaction. *Okeanologia* **22**, 711–718 (Engl. transl. *Oceanology* **22**, 525–530).

Makin, V. K. 1983*a* On wind energy transfer to surface gravity waves. *Okeanologia* **23**, 711–718 (Engl. transl. *Oceanology* **23**, 424–428).

Makin, V. K. 1983*b* Effect of stratification of an atmospheric layer over a water surface on the energy flux to the waves. *Izv. Akad. Nauk. SSSR. Atmos. Ocean. Phys.* **19**, 765–767 (Engl. transl. *Izv. Atmos. Ocean. Phys.* **19**, 574–576).

Makin, V. K. & Chalikov, D. V. 1980 Laboratory studies of wind waves. *Okeanologia* **20**, 806–817 (Engl. transl. *Oceanology* **20**, 531–537).

Miles, J. W. 1957 On the generation of surface waves by shear flows. *J. Fluid Mech.* **3**, 185–204.

Miles, J. W. 1959 On the generation of surface waves by shear flows. Part 2. *J. Fluid Mech.* **6**, 568–582.

Miles, J. W. 1967 On the generation of surface waves by shear flows. Part 5. *J. Fluid Mech.* **30**, 163–175.

Mitsuyasu, H. & Honda, T. 1982 Wind-induced growth of water waves. *J. Fluid Mech.* **151**, 427–442.

Mitsuyasu, H., Tasai, F., Suhara, T., Mizuno, S., Ohkuso, M., Honda, T. & Rikiishi, K. 1975 Observations of the directional spectrum of ocean waves using a cloverleaf buoy. *J. Phys. Oceanogr.* **5**, 750–760.

Müller, P., Olbers, D. J. & Willebrand, J. 1978 The IWEX spectrum. *J. Geophys. Res.* **83**, 479–499.

Munk, W. H., Miller, G. R., Snodgrass, F. E. & Barber, N. F. 1963 Directional recording of swell from distant storms. *Phil. Trans. R. Soc. Lond.* A **255**, 505–584.

Papadimitrakis, Y. A., Hsu, E. Y. & Street, R. L. 1985 On the resolution of organized spurious pressure fluctuations in wind-wave facilities. *J. Acoust. Soc. Am.* **77**, 896–906.

Papadimitrakis, Y. A., Hsu, E. Y. & Street, R. L. 1986 The role of wave-induced pressure fluctuations in the transfer processes across an air–water interface. *J. Fluid Mech.* **170**, 113–137.

Papadimitrakis, Y. A., Street, R. L. & Hsu, E. Y. 1988 The bursting sequence in the turbulent boundary layer over progressive, mechanically generated water waves. *J. Fluid Mech.* **193**, 303–345.

Phillips, O. M. 1957 On the generation of waves by turbulent wind. *J. Fluid Mech.* **2**, 417–445.

Plant, W. J. 1982 A relationship between wind stress and wave slope. *J. Geophys. Res.* **87**, 1961–1967.

Shemdin, O. H. & Hsu, E. Y. 1967 Direct measurement of aerodynamic pressure above a simple progressive gravity wave. *J. Fluid Mech.* **30**, 403–416.

Snodgrass, F. W., Groves, G. W., Hasselmann, K. F., Miller, G. R., Munk, W. H. & Powers, W. H. 1966 Propagation of ocean swell across the Pacific. *Phil. Trans. R. Soc. Lond.* A **259**, 431–497.

Snyder, R. L. 1974 A field study of wave-induced pressure fluctuations above surface gravity waves. *J. Mar. Res.* **32**, 497–531.

Snyder, R. L., Dobson, F. W., Elliott, J. A. & Long, R. B. 1981 Array measurements of atmospheric pressure fluctuations above surface gravity waves. *J. Fluid Mech.* **102**, 1–59.

Snyder, R. L., Long, R. B., Irish, J., Hunley, D. G. & Pflaum, N. C. 1974 An instrument to

measure atmospheric pressure fluctuations above surface gravity waves. *J. Mar. Res.* **32**, 485–496.

STEWART, R. H. 1970 Laboratory studies of the velocity field over deep-water waves. *J. Fluid Mech.* **42**, 733–754.

STEWART, R. W. 1974 The air–sea momentum exchange. *Boundary-Layer Met.* **6**, 151–167.

TAKEUCHI, K., LEAVITT, E. & CHAO, S. P. 1977 Effects of water waves on the structure of turbulent shear flow. *J. Fluid Mech.* **80**, 535–559.

TOWNSEND, A. A. 1972 Flow in a deep turbulent boundary layer over a surface distorted by water waves. *J. Fluid Mech.* **55**, 719–735.

TOWNSEND, A. A. 1980 The response of sheared turbulence to additional distortion. *J. Fluid Mech.* **81**, 171–191.

WU, J. 1982 Wind stress coefficients over sea surface from breeze to hurricane. *J. Geophys. Res.* **87**, 9704–9706.

YOUNG, I. R. & SOBEY, R. J. 1985 Measurements of the wind-wave energy flux in an opposing wind. *J. Fluid Mech.* **123**, 427–442.